NUREGCR4694

ornl

NUREG/CR-4694
ORNL/TM-9905

OAK RIDGE NATIONAL LABORATORY

MARTIN MARIETTA

Application of THERMIX-KONVEK Code to Accident Analyses of Modular Pebble Bed High Temperature Reactors (HTRs)

J. C. Cleveland
S. R. Greene

Work Performed for
U.S. Nuclear Regulatory Commission
under
DOE Interagency Agreement No. 40-544-75

OPERATED BY
MARTIN MARIETTA ENERGY SYSTEMS, INC.
FOR THE UNITED STATES
DEPARTMENT OF ENERGY

Available from

Superintendent of Documents
U.S. Government Printing Office
Post Office Box 37082
Washington, D.C. 20013-7982

and

National Technical Information Service
Springfield, VA 22161

NUREG/CR-4694
ORNL/TM-9905
Dist. Category R8

Engineering Technology Division

APPLICATION OF THERMIX-KONVEK CODE TO ACCIDENT ANALYSES OF MODULAR PEBBLE BED HIGH TEMPERATURE REACTORS (HTRs)

J. C. Cleveland
S. R. Greene

Manuscript Completed — July 29, 1986
Date Published — August 1986

Work Performed for
U.S. Nuclear Regulatory Commission
under
DOE Interagency Agreement No. 40-544-75
NRC FIN No. A9473

Prepared by the
OAK RIDGE NATIONAL LABORATORY
Oak Ridge, Tennessee 37831
operated by
MARTIN MARIETTA ENERGY SYSTEMS, INC.
for the
U.S. DEPARTMENT OF ENERGY
under Contract No. DE-AC05-840R21400

CONTENTS

ACKNOWLEDGMENT

The cooperation of the German Ministry for Research and Technology (BMFT) in releasing THERMIX-KONVEK for safety studies of HTRs under the USNRC program within the frame of the Technical Exchange and Cooperative Agreement between the USNRC and the BMFT in the field of Reactor Safety Research and Development is sincerely appreciated. The cooperation of the Kernforschungsanlage-Jülich in providing THERMIX-KONVEK, its documentation, sample problems and code validation reports to ORNL and for reviewing this report is also sincerely appreciated.

APPLICATION OF THERMIX-KONVEK CODE TO ACCIDENT ANALYSES OF MODULAR PEBBLE BED HIGH TEMPERATURE REACTORS (HTRs)

J. C. Cleveland
S. R. Greene

ABSTRACT

The THERMIX-KONVEK code was used to model the steady state and dynamic thermal behavior of the U.S. pebble bed modular HTR concept and trial calculations for accident conditions were performed. Results of these trial calculations are compared with other predictions by ORNL and by industrial proponents.

The basic equations, assumptions, and calculational technique employed in THERMIX-KONVEK are presented. Code validation efforts conducted at Kernforschungsanlage-Jülich (KFA) are summarized, and the applicability of the code to the U.S. pebble bed modular HTR is assessed.

It was concluded that the code is applicable to analyses of the safety behavior of the U.S. modular pebble bed HTR. Significant code validation has been conducted using out-of-reactor test loops at KFA. Predicted results agree well with measured data except for test conditions leading to asymmetric behavior which cannot be predicted with the two-dimensional THERMIX-KONVEK model. Suggestions are made for additional code development including comparison of code predictions with reactor operating data.

---

1. INTRODUCTION

This report presents results of ORNL's initial application of the THERMIX-KONVEK thermal fluid dynamic code to accident analyses of the pebble bed modular High Temperature Reactor (HTR). The code has been developed by Kernforschungsanlage Jülich (KFA) during the past ten years and is used in Germany for reactor design and licensing assessments of pebble bed reactors. THERMIX-KONVEK was released for safety studies of HTRs under the USNRC program by the German Ministry for Research and Technology (BMFT) within the frame of the Technical Exchange and Cooperative Agreement between the USNRC and the BMFT in the field of Reactor Safety Research and Development.

The objectives of this initial effort have been to

(1) develop a model of the U.S. pebble bed modular HTR and complete initial trial calculations of loss of flow and loss of heat sink accidents, and if possible, reactivity insertion accidents.

(2) assess code development and validation needs.

This report summarizes the basic assumptions and calculational techniques used in THERMIX-KONVEK. A model of the U.S. modular pebble bed reactor was developed and initial calculations for a loss of flow and loss of heat sink accident and for a depressurized core heatup accident are reported. Results are compared with other results available for pebble bed modular HTRs.

The existing THERMIX-KONVEK validation work has been summarized and assessed relative to application of the code to the U.S. modular pebble bed reactor concept. Recommended steps for additional validation are presented. Finally, recommendations for additional analyses of modular HTRs are presented and required code development efforts are discussed.

A request to KFA has been made for the KINEX neutron kinetics module of THERMIX which provides the capability for analyses of reactivity insertion transients. A suggested next step in ORNL's application of the code involves trial calculations of reactivity insertion transients using KINEX coupled to THERMIX-KONVEK.

2. SUMMARY OF MODELING APPROACH, ASSUMPTIONS, AND CALCULATIONAL TECHNIQUE

THERMIX-KONVEK calculates the temperature and flow conditions within the pebble bed HTR for steady state conditions and for transient conditions which follow shutdown of the reactor. The KINEX module couples with THERMIX-KONVEK to perform neutron kinetics calculations required for analyses of "at power" transients including changes in reactivity. Different aspects of the THERMIX-KONVEK modeling approach, assumptions, and calculational technique are presented in Refs. 1-3. Because this documentation is spread out and incomplete, the following description of the THERMIX-KONVEK modeling technique has been written as a first step to bring together a more complete description of the modeling approach and to fill in certain gaps not explicitly discussed in the existing documentation.

The pebble bed thermal fluid dynamic model is based on representations of the solid and of the flowing fluid as follows:

- heat transfer and heat storage in the pebble bed are considered on a two-dimensional macroscopic scale for partial bed volumes;
- the temperature distribution within representative individual fuel pebbles at specified locations is computed;
- the coolant gas flow is treated as two-dimensional flow through a porous media.

The calculation of temperatures within the pebble bed, and of temperatures within representative individual pebbles, is coupled to the calculation of the gas flow and temperature distribution as shown in Fig. 2.1.

2.1 Basic Equations for Modeling Solid and Gas

The basic equations which are solved by THERMIX-KONVEK are presented below, and the sections which follow provide a summary of the solution technique.

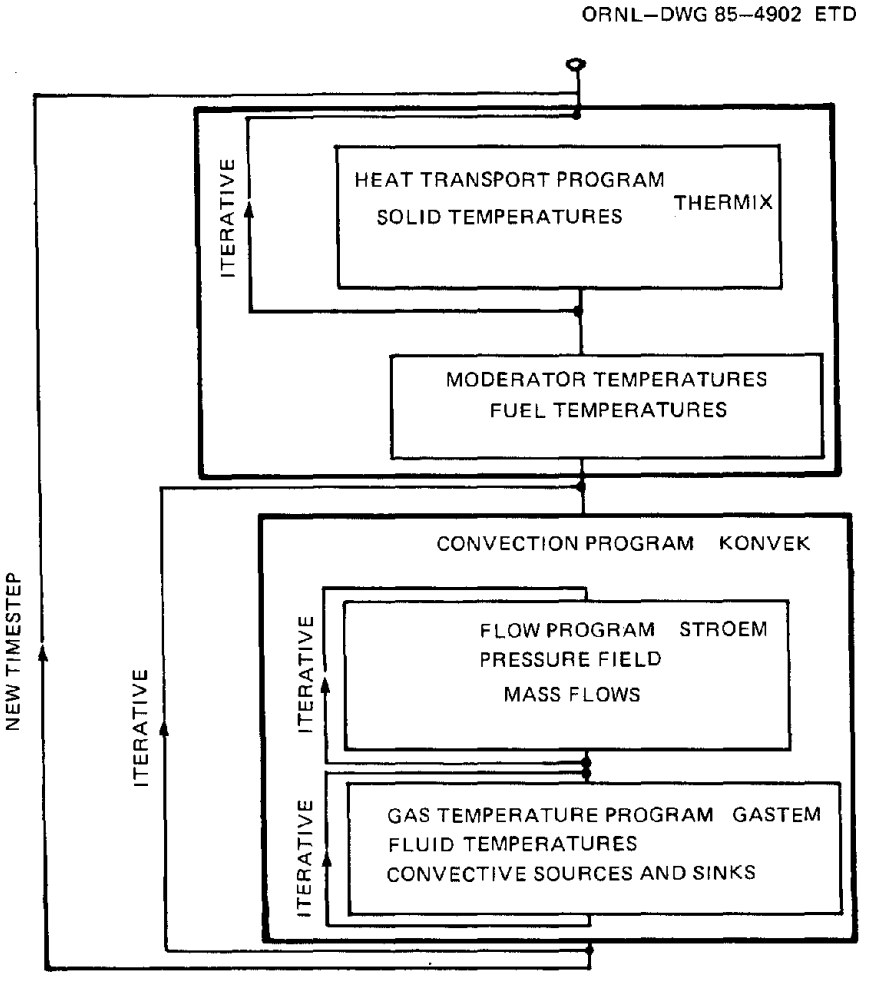

Fig. 2.1. Flow scheme for the THERMIX-KONVEK code. (Figure taken from Ref. 2.)

2.1.1 Pebble bed temperature distribution (two-dimensional, r-z, macroscopic representation of the temperature distribution within the pebble bed)

Conservation of energy, dynamic representation:

$$\rho c_p \frac{\partial T}{\partial t} = \frac{1}{r}\frac{\partial}{\partial r}\left(r\,\lambda_e \frac{\partial T}{\partial r}\right) + \frac{\partial}{\partial z}\left(\lambda_e \frac{\partial T}{\partial z}\right) + \dot{q}_n''' + \dot{q}_k''' \quad , \qquad \text{(Eq. 1)}$$

where r,z are the coordinates of a point in the pebble bed, and

T = bed temperature

ρc_p = volumetric heat capacity of homogenized bed

λ_e = effective bed conductivity (which includes thermal conduction and radiation) independent of coolant flow

$\dot{q}_n'''$ = nuclear heat source rate density

$\dot{q}_k'''$ = convective heat source (sink) rate density.

2.1.2 Temperature distribution within the pebbles (radially symmetric, one dimensional, temperature distribution within the pebble)

Conservation of energy, dynamic representation:

$$\rho c_p \frac{\partial T}{\partial t} = \frac{1}{R^2} \frac{\partial}{\partial R} \left(R^2 k \frac{\partial T}{\partial R} \right) + \dot{q}_n''' \quad , \qquad \text{(Eq. 2)}$$

where

$\dot{q}_n'''$ is the nuclear heat source rate density

R = distance from pebble center

k = pebble conductivity

ρc_p = pebble volumetric heat capacity.

2.1.3 Gas temperature and flow distribution (2 dimensional, r-z quasi-static representation of pressure and flow field)

Conservation of mass: quasi-static representation ($\nabla \cdot \vec{G} = \phi$)

$$\frac{1}{r} \frac{\partial}{\partial r} (r\, G_r) + \frac{\partial}{\partial z} G_z = \phi \quad , \qquad \text{(Eq. 3)}$$

where G_r and G_z are the components of the flow vector $\vec{G}$. (G has units $kg/s/m^2$.) $\vec{G} = \rho \vec{v}$, and

ϕ = mass source rate density ($kg/s/m^3$) (e.g. mass source introduced into lower plenum).

Note that time dependent mass storage is neglected in Eq. 3.

Conservation of momentum, quasi-static representation neglecting inertia and spatial acceleration:

$$\nabla P + \vec{R} - \rho \vec{g} = 0, \quad \text{or}$$

$$\frac{\partial P}{\partial r} + \frac{\psi}{d} \frac{1 - \varepsilon}{\varepsilon^3} \frac{|G|}{2\rho} G_r = 0 \qquad \text{(Eq. 4a)}$$

and

$$\frac{\partial P}{\partial z} + \frac{\psi}{d} \frac{1 - \varepsilon}{\varepsilon^3} \frac{|G|}{2\rho} G_z - \rho g = 0 \quad , \qquad \text{(Eq. 4b)}$$

where

$\vec{R}$ = frictional force per unit volume and, according to Ref. 4, is represented as

$$\vec{R} = \frac{\psi}{d} \frac{1 - \varepsilon}{\varepsilon^3} \frac{|G|}{2\rho} \vec{G}$$

P = static pressure

ρ = gas density

ψ = pressure loss coefficient for flow through pebble bed (given in Ref. 4 as a function of the Reynolds number)

d = pebble diameter.

Conservation of energy, quasi-static representation: Given the solid body temperature distribution and the gas flow field (from Eqs. 3, 4a and 4b) the gas temperature field is determined by:

$$c_p \nabla \cdot (T_g \vec{G}) = \nabla \cdot (\lambda^* \nabla T_g) + c_p \phi T_{source}$$

or

$$c_p \frac{1}{r} \frac{\partial}{\partial r} (r T_g G_r) + c_p \frac{\partial}{\partial z} (T_g G_z) = \frac{1}{r} \frac{\partial}{\partial r} \left(r \lambda^* \frac{\partial T_g}{\partial r} \right) + \frac{\partial}{\partial z} \left(\lambda^* \frac{\partial T_g}{\partial z} \right)$$

$$+ c_p \phi T_{source} , \qquad \text{(Eq. 5)}$$

where

T_g = gas temperature

λ^* = effective thermal conductivity of the gas due to dispersion

c_p = gas specific heat capacity

T_{source} = temperature of gas source

ϕ = mass source rate density.

The terms on the left hand side of the above equation represent the convective heat transport rate while the terms on the right represent the dispersive heat transport rate, and the rate of energy introduction by a mass source. Note that time dependent energy storage terms and compressive work terms are neglected.

The dispersive heat transfer is a function of local conditions and is treated by means of an effective thermal conduction. In the flow direction it is generally negligible relative to the convective heat flow.

As discussed above, the gas temperature, flow, and pressure fields are obtained by solving the steady state quasi-static form of the equations for conservation of energy, mass, and momentum. Mass storage effects due to the variation of the gas density profile over time are disregarded. This is permissible because

- the heat storage in the coolant gas is not significant compared with heat storage in the solid, and thus changes in mass content of a given fluid node need not be computed to formulate the energy balance; and
- changes in gas density resulting from changes in solid temperature occur slowly due to slow changes in solid temperature.

The following simple example illustrates the unimportance of energy storage in the helium for the determination of core temperatures (even in the depressurized case). Consider 1 m^3 of a pebble bed core with the helium content initially at 750°C and 70 bar. The helium volume is 0.39 m^3 (the pebble bed void fraction). A 500°C decrease in helium temperature results in a decrease in helium internal energy of 1.8 MJ. If the pressure also drops to 1 bar, the internal energy change of the helium in the 1 m^3 of core volume is 2.2 MJ. However, a 500°C drop in the solid temperature (for example from 1000°C to 500°C) results in a change in energy storage in the solid of 1200 MJ; thus the energy change of the gas has an insignificant effect on solid temperature.

In the conservation of momentum equation for the gas flow through the pebble bed (Eq. 4), acceleration losses are neglected. The insignificance of acceleration losses through the pebble bed relative to frictional losses can be seen by the following example using modular HTR conditions. The pressure loss due to gas acceleration through the bed is

$$\Delta P_a = \left(\frac{G}{\varepsilon}\right)^2 \left(\frac{1}{\rho_{out}} - \frac{1}{\rho_{in}}\right) .$$

Frictional losses in the bed can be represented as (see Section 2.1.3)

$$\frac{\Delta P_f}{\Delta H} = \psi \frac{1-\varepsilon}{\varepsilon^3} \frac{1}{d} \frac{1}{2\rho} G^2 ,$$

where ψ is a function of Reynolds number. For modular HTR full flow conditions, ψ is fairly constant through the core ranging from 2.0 at the core inlet to 2.1 at the core outlet. Using 2 as an approximate value for ψ and integrating over core height gives

$$\Delta P_f \approx (2) \frac{1-\varepsilon}{\varepsilon} \frac{1}{d} \left(\frac{G}{\varepsilon}\right)^2 \frac{1}{2} \frac{H}{(\rho_{out} - \rho_{in})} \ln (\rho_{out}/\rho_{in}) ,$$

where it has been assumed that the gas density varies linearly with distance through the core. For full flow conditions in the U.S. pebble bed modular HTR, the above relationships give

$$\Delta P_f \approx 500 \, \Delta P_a .$$

Clearly, at full flow conditions, acceleration losses in the bed can be neglected. For natural convection conditions (both pressurized and depressurized) neglecting acceleration losses is even more accurate since ψ increases with decreasing Reynolds number.

To a close approximation the flow is in equilibrium with the driving pressure differences, since friction accounts for the largest portion of the pressure drop and acceleration losses are small. Thus the inertial term in the momentum equation is small and is neglected in THERMIX-KONVEK allowing the flow to be calculated in steady state (see Eq. 4).

2.2 Solution Technique for Temperature Distribution Within the Pebble Bed

2.2.1 Discretization of heat transport equation

To solve for the macroscopic temperature distribution within the pebble bed, Eq. 1 is multiplied by the volume element $dV = 2\pi r \, dr \, dz$,

and the term r $\partial T/\partial r$ is represented as $\partial T/\partial(\ln r)$ to give

$$\rho\, c_p \frac{\partial T}{\partial t}\, dV = 2\pi \frac{\partial}{\partial r}\left(\lambda_e \frac{\partial T}{\partial \ln r}\right) dr\, dz + \frac{\partial}{\partial z}\left(\lambda_e \frac{\partial T}{\partial z}\right) 2\pi r\, dr\, dz + (\dot{q}'''_n + \dot{q}'''_k)\, dV .$$

This equation is then integrated over the volume element shown in Fig. 2.2. The volume integrals of the first two terms on the right hand side of the above equation are treated as follows:

$$\iint 2\pi \frac{\partial}{\partial r}\left(\lambda_e \frac{\partial T}{\partial \ln r}\right) dr\, dz = 2\pi \int \left[\lambda_e \frac{\partial T}{\partial \ln r}\right]\Big|_{r_{in}}^{r_{out}} dz$$

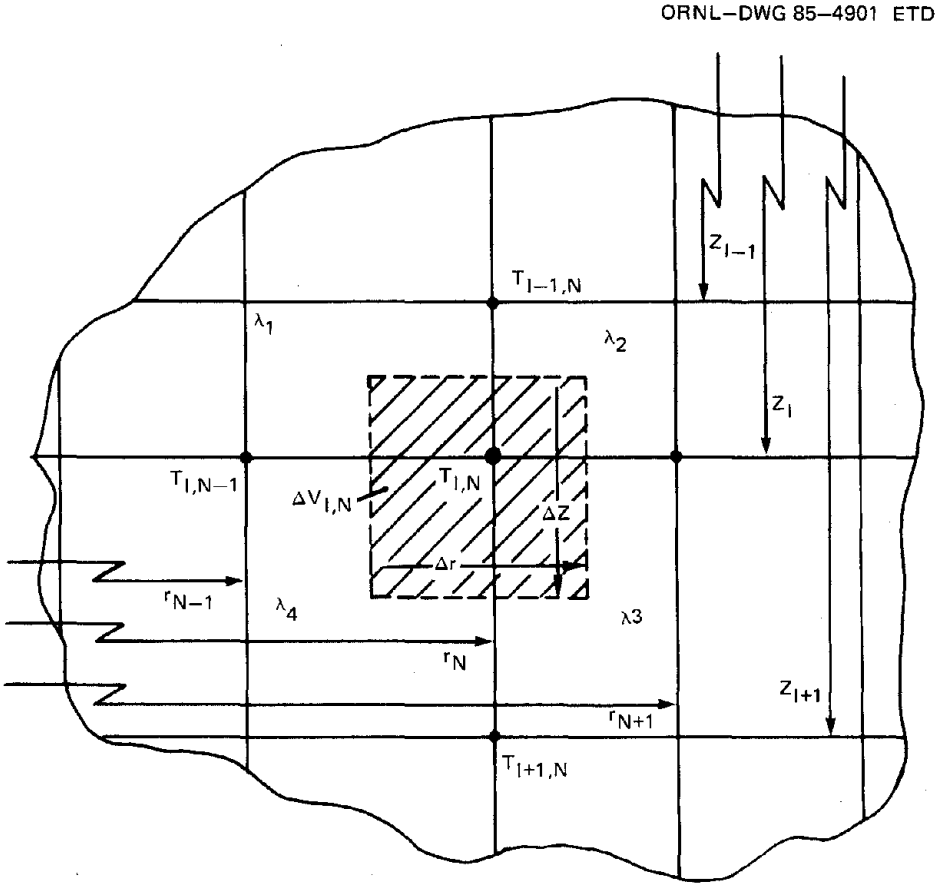

Fig. 2.2. Spatial discretization of the solid model. (Figure taken from Ref. 1.)

and

$$\iint 2\pi r \frac{\partial}{\partial z}\left(\lambda_e \frac{\partial T}{\partial z}\right) dz\, dr = 2\pi \int r \left[\lambda_e \frac{\partial T}{\partial z}\right]\Big|_{z_{bottom}}^{z_{top}} dr ,$$

where r_{in} and r_{out} are the inner and outer radii of the volume element and z_{bottom} and z_{top} are the distances to the bottom and top of the volume element shown in Fig. 2.2. Then

$$2\pi \int \left[\lambda_e \frac{\partial T}{\partial \ell n\, r}\right]\Big|_{r_{in}}^{r_{out}} dz = 2\pi \Delta z \quad \lambda_{e,\overline{23}} \frac{T_{I,N+1} - T_{I,N}}{\ell n\,(r_{N+1}/r_N)}$$

$$- \lambda_{e,\overline{14}} \frac{T_{I,N} - T_{I,N-1}}{\ell n\,(r_N/r_{N-1})}$$

and

$$2\pi \int r \left(\lambda_e \frac{\partial T}{\partial z}\right)\Big|_{z_{bottom}}^{z_{top}} dr = 2\pi\, r_N\, \Delta r \quad \lambda_{e,\overline{12}} \frac{T_{I-1,N} - T_{I,N}}{z_{I-1} - z_I}$$

$$- \lambda_{e,\overline{13}} \frac{T_{I,N} - T_{I+1,N}}{z_I - z_{I+1}} ,$$

where, for example

$$\lambda_{e,\overline{23}} = \frac{\lambda_{e,2}\,(z_I - z_{I-1}) + \lambda_{e,3}\,(z_{I+1} - z_I)}{z_{I+1} - z_{I-1}} .$$

Having performed the spatial integration yielding the lumped node model, an integration over time is carried out according to the Crank-Nicolson procedure. The heat transport equation is written for time $t^{j+1/2} \equiv (t^{j+1} + t^j)/2$ where t^{j+1} represents the new time at which the temperature field is to be calculated and t^j represents the old time at which all temperatures are known. The following approximations are made:

$$\left.\frac{dT_{I,N}}{dt}\right|_{t^{j+1/2}} \doteq \frac{T_{I,N}^{j+1} - T_{I,N}^{j}}{\Delta t^j} \qquad (\Delta t^j \equiv t^{j+1} - t^j)$$

and all temperatures and source densities on the right hand side of the heat conduction equation at time $t^{j+1/2}$ are approximated by their average value during Δt^j; for example

$$T\left(t^{j+1/2}\right)_{I-1,N} \doteq \frac{T^j_{I-1,N} + T^{j+1}_{I-1,N}}{2} .$$

This results in a set of IMAX * NMAX algebraic equations involving the unknown nodal temperatures at the future time (t^{j+1}) and known nodal temperatures at time t^j:

$$(\rho c_p)_{I,N}\, 2\pi r_N\, \Delta r_N\, \Delta z_I \frac{T^{j+1}_{I,N} - T^j_{I,N}}{\Delta t^j} =$$

$$2\pi\, \Delta z_I \quad \lambda_{e,\overline{23}} \frac{T^{j+1}_{I,N+1} + T^j_{I,N+1} - T^{j+1}_{I,N} - T^j_{I,N}}{2\, \ell n\, (r_{N+1}/r_N)} + \ldots \quad + \ldots$$

$$+ \pi r_N\, \Delta r_N\, \Delta z_I \quad [\dot{q}'''^{(j+1)}_{I,N} + \dot{q}'''^{(j)}_{I,N}] .$$

This set of equations has temperature dependent coefficients. These equations are solved iteratively for the nodal temperatures at the future time by means of a point relaxation method with successive over-relaxation.

Future evaluations of the code (item 5 of Section 7 of this report) need to examine how the convective heat source, $\dot{q}'''_k$, at time t^{j+1} is estimated in order for the code to compute the solid temperatures at time t^{j+1}. This is not clear from the existing documentation or from the computational flow diagram of Fig. 2.1.

At the centerline (r = 0) the boundary condition that $\frac{dT}{dr} = 0$ is applied. Future evaluations of the code need to examine how this is incorporated into the above heat transfer equation.

This homogenized pebble bed thermal model determines a local temperature value for each volume element in the macroscopic mesh. The resulting temperatures of the homogenized bed volume are representative of fuel temperatures for conditions involving small temperature gradients

within the individual fuel pebbles. For analyses of "at power" transient conditions, for which there are significant temperature gradients within the pebbles, a heterogeneous pebble model is provided to compute the temperature distribution within representative pebbles at specified locations within the pebble bed.

2.2.2 Pebble bed effective thermal conductivity:

In Eq. 1, λ_e represents the effective thermal conductivity for the pebble bed. It accounts for the following heat transport mechanisms:

1) Thermal conduction through the pebble
2) Thermal conduction through the contact points
3) Thermal conduction from solid to fluid to solid
4) Radiation between facing pebbles

The version of THERMIX-KONVEK provided by KFA to ORNL represents λ_e with the correlation

$$\lambda_e = (1.9 \times 10^{-5})\ (T - 150)^{1.29} \ , \qquad \text{(Eq. 6)}$$

where T = local solid temperature (°C), and λ_e is in W/cm K. Ref. 1 presents a somewhat different correlation [$\lambda_e = 2.0 \times 10^{-5}(T-135)^{1.29} + 0.003$] which apparently was used in earlier versions of THERMIX. See Section 5.1.1 for a discussion of KFA efforts to experimentally determine correlations for λ_e and to obtain analytical formulations for λ_e.

2.3 Solution Technique for Temperature Distribution Within Fuel Pebbles

At selected locations within the pebble bed, a heterogeneous pebble model is provided. Temperatures of each of five spherical shells within the pebble are determined numerically from Eq. 2. Heat generation in the individual fuel microspheres is homogenized within the fueled zone of the pebble. The following boundary conditions are applied to Eq. 2:

$$\text{at } R = 0, \ \frac{\partial T}{\partial R} = 0 \text{ (where R is the distance from the pebble center)}$$

$$\text{at } R = R_p, \ 4 \pi R_p^2 k \frac{\partial T}{\partial R} = (\dot{Q}_{\lambda s} + \dot{Q}_k) \ ,$$

where $\dot{Q}_k$ represents the rate of heat removal from the pebble by convection and $\dot{Q}_{\lambda s}$ is the rate of heat removal from the pebble due to the effective conductivity within the bed. [Note that the two means of heat removal from the pebble surface ($R = R_p$) are by convection and by an effective conduction (which includes radiation) through the bed.] $\dot{Q}_{\lambda s}$ is determined from the effective conductivity, λ_e, and the temperature field of the macroscopic mesh used in the homogeneous bed model. $\dot{Q}_{\lambda s}$ is obtained as follows: The net rate of heat flowing into the control element of the macroscopic mesh shown in Fig. 2.3 in which the pebble is located is represented as

$$\int \lambda_e \nabla T \cdot d\vec{A} = \int \nabla \cdot (\lambda_e \nabla T)\, dV ,$$

where $dV = 2\pi r\, dr\, dz$ and the integration is carried out over the macroscopic control element whose volume is ΔV. Since $\dot{Q}_{\lambda s}$ is the fraction of this heat flowing into one pebble in the macroscopic control element and the control element contains N_p pebbles

$$\dot{Q}_{\lambda s} = \frac{1}{N_p} \int \nabla \cdot (\lambda_e \nabla T)\, dV$$

and

$$N_p = \Delta V\ (1 - \varepsilon)/V_{pebble} .$$

Performing this integration over the control element shown in Fig. 2.3 gives

$$\dot{Q}_{\lambda s} = \left(\lambda_{e,r_2} \frac{T_{r_2} - T}{\ln(r_2/r)} + \lambda_{e,r_1} \frac{T_{r_1} - T}{\ln(r/r_1)} \right) 2\pi\, \Delta z + \sum_{i=1}^{2} \lambda_{e,z_i} \frac{T_{z_i} - T}{|z_i - z|} \cdot A_z \Bigg) \frac{V_{pebble}}{\Delta V\ (1 - \varepsilon)} .$$

To solve for the temperature of the pebble shells Eq. 2 is integrated over each shell (see Fig. 2.3) resulting in, for the kth pebble

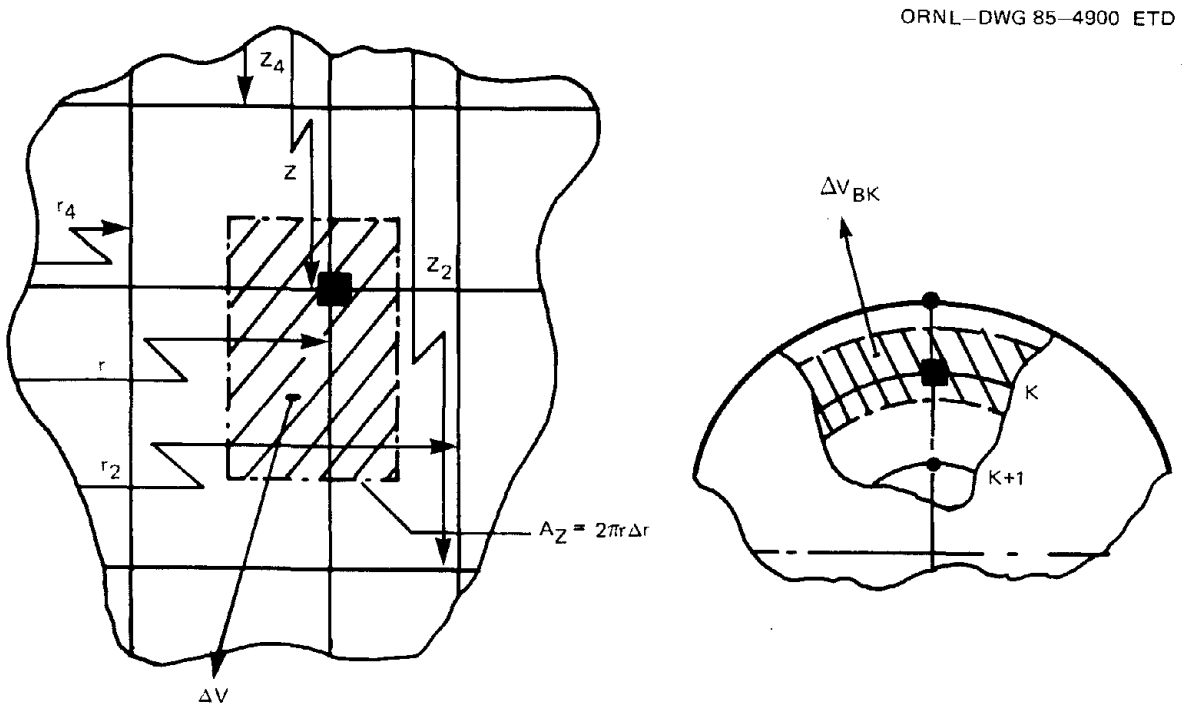

Fig. 2.3. (a) Discretization of the homogenized pebble bed in cylindrical coordinates; (b) spherically symmetric discretization of the fuel element. (Figure taken from Ref. 2.)

shell

$$(\rho c)\ \Delta V \frac{dT_k}{dt} = W_k\ (T_{k+1} - T_k) + W_{k-1}\ (T_{k-1} - T_k) + \dot{q}'''_n\ \Delta V\ ,$$

where W_k and W_{k+1} are conductance terms: $W_k = 4\pi R_k^2 k/(R_{k-1} - R_k)$. The derivative term is represented by

$$\frac{dT_k}{dt} \doteq \frac{T_k^{j+1} - T_k^j}{\Delta t^j}\ ,$$

where T_k^{j+1} is the temperature of the kth pebble shell at the new time, t_{j+1}, and T_k^j is the temperature of the kth pebble shell at the old time, t_j. The integration is performed either by iteration or by matrix solution as requested by the user.

2.4 Solution Technique for Fluid Conditions

2.4.1 Quasi-static representation of fluid

The pebble bed flow field model applies to a sufficiently large nonordered bed of equal diameter pebbles treated as a homogeneous porous solid. The condition of the gas is described by vector flow velocities and mass fluxes and by a macroscopic pressure field and a macroscopic temperature field. The following technique is used to obtain the gas flow and temperature distribution:

a. Based on estimated gas temperatures, a flow field is determined.

b. From the resultant flow field and from the solid surface temperatures resulting from the THERMIX computation, a new gas temperature field is computed.

c. The flow field calculation is repeated and the procedure continues until convergence is achieved.

To solve for the flow and pressure fields the conservation of mass and momentum equations (Eqs. 3 and 4) are integrated over the mesh volume of Fig. 2.4. The spatial derivatives of pressure in Eq. 4 are represented by a central difference and a system of IMAX × NMAX coupled algebraic equations for the pressure field is obtained. The system of equations is solved by an iterative point-relaxation method with successive over-relaxation. After each iteration the friction loss coefficients are recomputed.

The set of equations is also used to determine flow in regions other than the bed region. Flow through vertical channels (e.g., in the side and bottom reflectors in the U.S. pebble bed modular HTR concept) is determined by setting radial flow resistance to infinity and using appropriate values for axial flow resistance. For cavities such as the upper and lower plena, the frictional loss is set to zero and a uniform pressure is assumed throughout the cavity. Circulation inside the plena, which can only be determined by solving the complete Navier-Stokes equation, consequently cannot be simulated with this model.

To solve the conservation of energy equation for the gas (Eq. 5) to obtain the gas temperature field, an early version of THERMIX used a

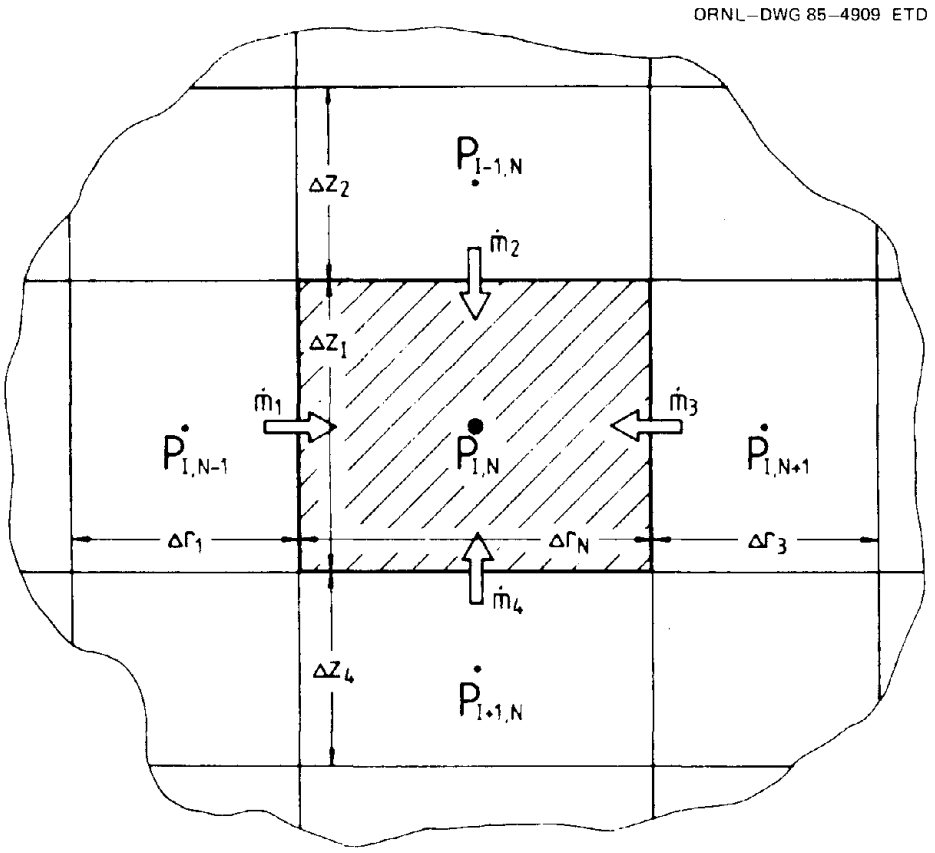

Fig. 2.4. Spatial discretization for the flow model. (Figure taken from Ref. 1.)

system of difference equations which was obtained by integration of Eq. 5 over a mesh volume in similar fashion to the integration performed to derive difference equations for the solid temperature distribution. This process was abandoned however because it led to improper temperature predictions where there were sharp gradients in gas temperature. That technique was replaced by a revised method described in detail in Ref. 2.

In summary, this revised method uses an "exponential approach technique" which is derived by considering the approach of the gas temperature to the solid temperature for radial and axial components of mass flow. The solid temperature is assumed to vary linearly between the two known values of surface temperature at adjacent nodes. The procedure for computing gas temperature is as follows: consider node B which sees

gas flows from neighboring nodes. The temperature of gas flowing from node A to node B (which are separated by a distance ℓ), is determined from the known mass flow $\dot{m}_i$ from A to B (obtained by solving the conservation of mass and momentum equations) by

$$\dot{m}_i \, c_p \, dT_{gas,i}(x) = \frac{hA}{\ell} \left[T_{surface}(x) - T_{gas,i}(x) \right] dx \ ,$$

where $T_{gas,i}(x)$ is the temperature at x of the gas in mass stream $\dot{m}_i$ flowing from node A to node B and x is the distance from node A. If

$$T_{surface}(x) = T^A_{surface} + \frac{T^B_{surface} - T^A_{surface}}{\ell} x$$

and

$$T_u(x) = T_{gas,i}(x) - T_{surface}(x) \ ,$$

the above equation becomes

$$\frac{dT_u(x)}{dx} + \frac{h\,A}{\dot{m}_i \, c_p} \frac{1}{\ell} T_u(x) = - \frac{(T^B_{surface} - T^A_{surface})}{\ell} \ .$$

Integrating this for $T_u(x)$ gives

$$T_u(x) = \left[T_u(x=0) + (T^B_{surface} - T^A_{surface}) \frac{\dot{m}_i \, c_p}{h\,A} \right] \exp \left[- \frac{h\,A}{\dot{m}_i \, c_p} \frac{x}{\ell} \right]$$

$$- (T^B_{surface} - T^A_{surface}) \frac{\dot{m}_i \, c_p}{h\,A} \ ,$$

and evaluating at $x = \ell$ gives the temperature of the mass stream $\dot{m}_i$ at node B (referenced to the surface temperature of node B).

Then an equation is written for the enthalpy of the gas "mixture" at node B by summing the enthalpies brought into "node" B by the various

mass streams and the enthalpies introduced into node B by dispersion and possible mass sources:

$$(\Sigma \dot{m}_i + \Sigma \dot{m}_{source})\, c_p\, T^B_{gas} = \Sigma \dot{m}_i\, c_p\, T_{gas,i}(x=\ell)$$

$$+ \Sigma \dot{Q}_{\lambda *} + \Sigma \dot{m}_{source}\, c_p\, T_{source} \cdot$$

Note that the time dependence of the energy storage is neglected.

This equation, together with above equations for $T_{gas,i}(x=\ell)$ for all the flow paths leading to node B, form a system of equations for the gas temperature field. This system is solved by an iterative procedure.

2.4.2 Effective conductivity of the fluid

The effective conductivity, λ^*, of the fluid (Eq. 5) is a characteristic of flow in beds and takes into account the heat transport through deflection of the fluid as it flows past the pebbles (turbulent flow). This is termed dispersion or dispersive thermal conductivity. According to Ref. 3, the effective conductivity of the fluid, λ^* in Eq. 5, is

$$\lambda^* = \lambda_G\, (Re \cdot Pr)/K\ , \qquad \text{(Eq. 7)}$$

where λ_G is the gas conductivity and K is an empirical constant. According to Ref. 5, the value of K is anisotropic, being smaller in the flow direction than in the direction transverse to the flow. However, since the dispersive conductivity acting in the flow direction is only of secondary significance relative to convective heat transport, a distinction is not made, and THERMIX-KONVEK applies the approximation that $K_\perp = K_\parallel$. Reference 5 presents a correlation for $K_\perp$ as

$$K_\perp = 8 \cdot [2 - (1 - 2d/D)^2]$$

where d is distance from the vessel wall and D is vessel diameter.

2.4.3 Helium equation of state

Based on review by the Kerntechnischer Ausschuss (KTA) (Ref. 6) the equation of state used in THERMIX-KONVEK is

$$\rho = 48.14 \frac{P}{T} \Bigg/ \left(1 + 0.4446 \frac{P}{T^{1.2}}\right) ,$$

with ρ in kg/m^3,

P in bar, and

T in K.

2.4.4 Pebble bed heat transfer coefficient

Based on review (Ref. 7) by KTA of experimental results by various investigators of heat transfer in pebble beds, heat transfer (for a bed of equal diameter pebbles) is computed by:

$$\dot{Q} = hA_p(T_p - T_{gas}) ,$$

where

T_p = surface temperature of a pebble in the pebble bed, and

$$h = \frac{Nu\lambda}{d} ,$$

with

λ = gas thermal conductivity

d = pebble diameter

and

$$Nu = 1.27 \frac{Pr^{0.333}}{\varepsilon^{1.18}} Re^{0.36} + 0.033 \frac{Pr^{0.5}}{\varepsilon^{1.07}} Re^{0.86}$$

where

$$Re = \frac{\dot{m}/A\ d}{\eta}$$

and

d = pebble diameter

$\dot{m}$ = total mass flow (kg/s)

A = empty-core cross sectional area

η = dynamic viscosity

Pr = Prandtl number

ε = void fraction of the pebble bed.

For each node the dynamic viscosity η and the gas thermal conductivity λ are computed at the average of the pebble surface temperature and the gas temperature. As presented in Ref. 7, the range of application for this correlation is

$100 < Re < 10^5$

$0.36 < \varepsilon < 0.42$

$D/d > 20$

$H > 4d$

where

D = bed diameter

H = bed height

The restriction on the diameter ratio D/d is lifted if, in place of average values for the void fraction and Reynolds number, local values are used.

According to Ref. 7, the uncertainty band of the above correlation for Nu is ±20% with a statistical certainty of 95%.

2.4.5 Pebble bed pressure drop

Based on review (Ref. 4) by KTA of experimental results obtained by various investigators the pressure drop in the pebble bed is determined according to

$$\frac{\Delta P}{\Delta H} = \Psi \frac{1-\varepsilon}{\varepsilon^3} \frac{1}{d} \frac{1}{2\rho} \left(\frac{\dot{m}}{A}\right)^2$$

with

$$\Psi = \frac{320}{\left(\frac{Re}{1-\varepsilon}\right)} + \frac{6}{\left(\frac{Re}{1-\varepsilon}\right)^{0.1}},$$

where

ρ = gas density

A = cross sectional area

ε = void fraction

$\dot{m}$ = mass flow rate.

For each node the dynamic viscosity used in computing the Reynolds number ($= \frac{(\dot{m}/A)d}{\eta}$) is computed at the arithmetic average of the gas and the pebble surface temperature. The density is computed at the gas temperature. Reference 4 gives an uncertainty band for the above correlation of ±15% with a statistical certainty of 95%.

3. MODEL OF U.S. MODULAR HTR

The THERMIX-KONVEK code actually consists of two separate modules: one, named THERMIX, performs the steady state and transient heat conduction calculations, and the other, KONVEK, performs the quasi-static convection calculations. The user of the code must input two distinct model topographies into the code, one of which is employed by the THERMIX module and the other by KONVEK. These two models are described in the following subsections.

The reactor design information (geometry and steady state core inlet temperature, pressure and flow rate) used in the THERMIX-KONVEK model of the U.S. pebble bed modular HTR concept were obtained from handouts provided to NRC at a briefing by the DOE HTR Program on July 31—August 1, 1985. Other information, such as axial power shape versus normalized core height, which was not provided for the U.S. concept, was taken from German information (for the Interatom pebble bed modular HTR) provided to ORNL in the THERMIX-KONVEK sample problem. Further, material properties (for example specific heats, conductivities, and emissivities) used in the ORNL model are those provided with THERMIX-KONVEK and its sample problem. KFA has noted that this information should be considered preliminary and, in some instances, more accurate representations would be required for detailed analyses. ORNL judges the information to be appropriate for this stage of our analyses. Figure 3.1 shows a schematic of the U.S. pebble bed modular HTR.

With loss of forced circulation (LOFC) because the steam generator is located below the core, the design does not encourage natural convection through the main loop. Further, there is a main loop shutoff valve located in the circulator inlet which is of the Fort St. Vrain self-actuating flapper type. With loss of circulator flow, this valve closes due to gravity. Therefore, in the analyses of events involving LOFC which are reported in the following sections, the assumption is made that after LOFC there is no net flow through the main loop. Natural convection within the region including the core and the upper and lower plena was computed by THERMIX-KONVEK.

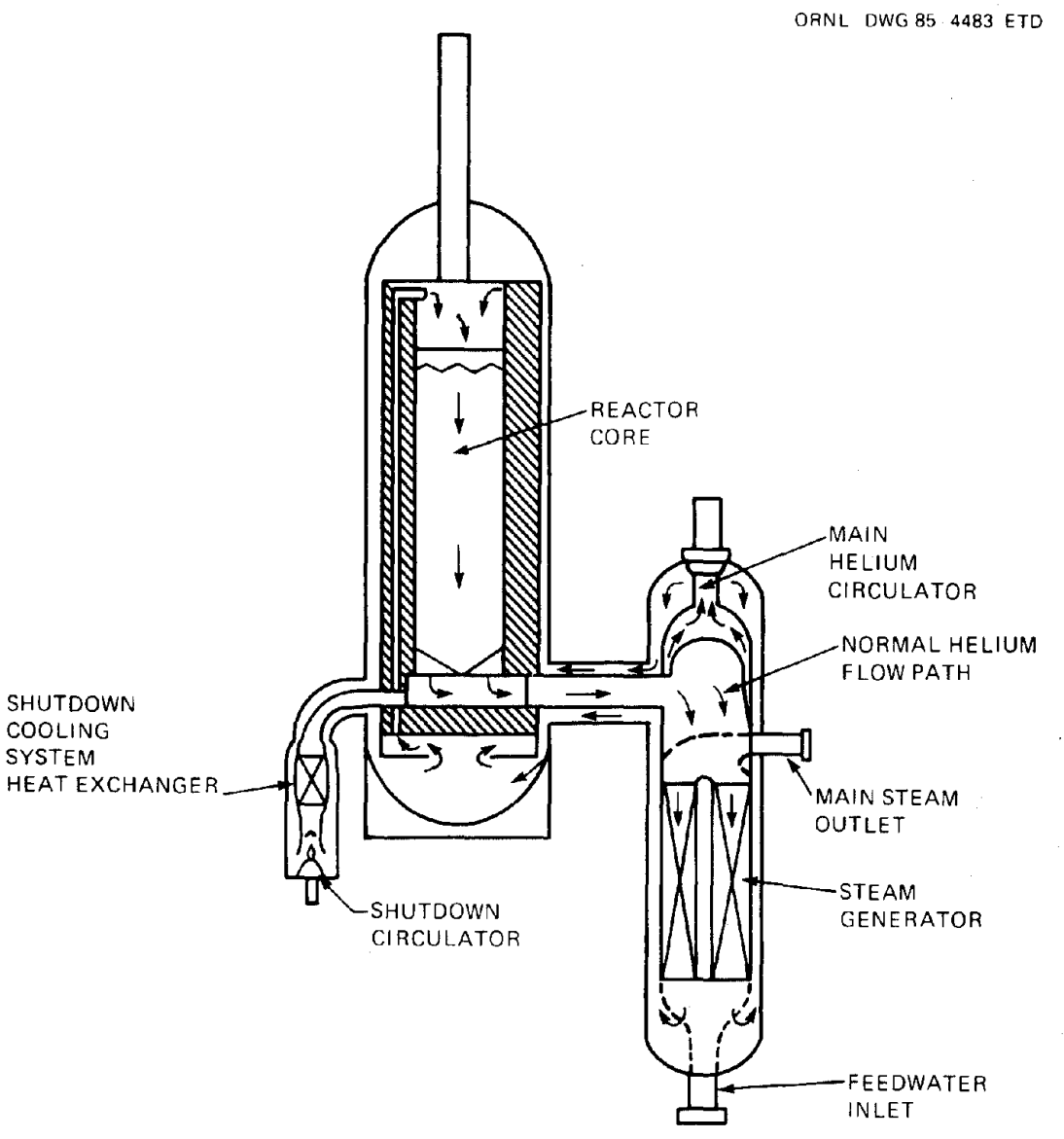

Fig. 3.1. Side-by-side steel vessel concept.

3.1 THERMIX Model

Figure 3.2 is a simplified schematic representation of the current ORNL THERMIX model of the U.S. side-by-side HTR. The two-dimensional model (r,z coordinate system) extends in the radial direction from the core center line to the reactor cavity wall, and in the axial direction from the upper reflector support plate to the lower core support plate.

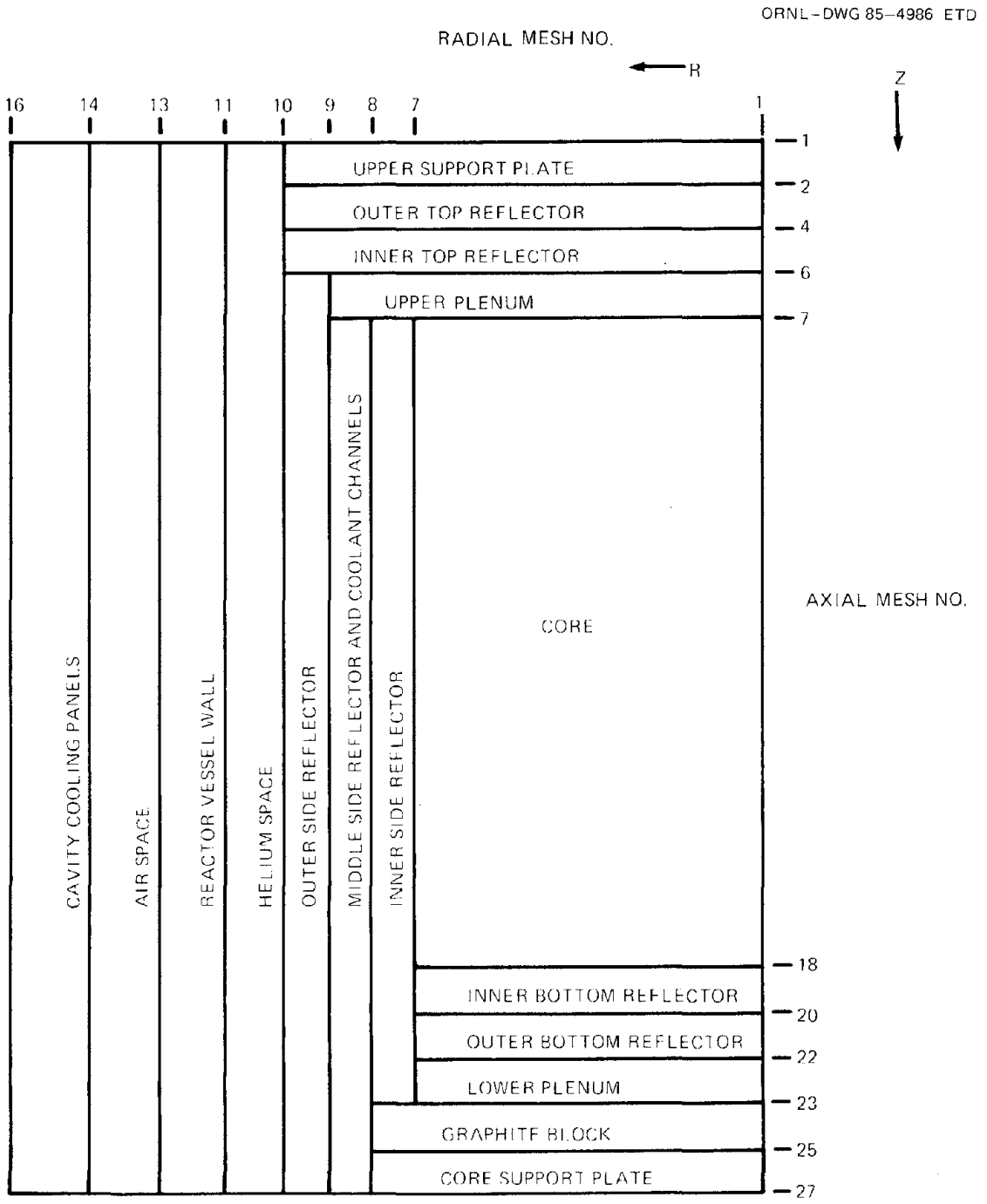

Fig. 3.2. Schematic representation of ORNL THERMIX model of U.S. pebble bed side-by-side modular HTR.

Although most of the major structural heat sinks which interact with the reactor core are included in the model, the two-dimensional nature of THERMIX does not facilitate any treatment of the core buttresses. A major simplification of this model is, therefore, that the core is treated as if the buttresses do not exist (i.e., the core is modeled as a perfect cylinder, with a height of 10.8 m and a diameter of 3 m).

The model is comprised of seventeen major zones of distinct composition. Zone 1 is the core, which is treated as a heterogeneous zone of fuel spheres. Zone 2 is the inner side reflector zone, which contains the control rods. Zone 3 is the middle side reflector zone which contains vertical channels in which the helium coolant flows in an upward direction through the graphite. Zone 4 is the outer side reflector zone. The gap between the reflector and the inner surface of the reactor vessel is treated by Zone 5, while the vessel wall itself is treated as Zone 6. Zone 7 represents the air gap between the outer surface of the reactor vessel and the reactor cavity cooling panels which are fixed to the vertical walls of the reactor cavity. Zone 8 represents the cavity cooling panels themselves, and functions as the outer radial boundary for the model.

Zone 9 represents the void space between the top of the fuel spheres and the bottom of the upper reflector. The upper reflector itself is divided into two zones, 10 and 11. The upper reflector support plate is designated Zone 12, and is treated as an adiabatic boundary. It should be noted that the configuration of the upper part of the THERMIX model is not identical to that of the actual design. In particular, the exact geometry of the upper plenum (the void space above the fuel spheres) and the pathways by which the helium coolant enters it cannot be simulated by the current version of THERMIX due to its inability to accommodate horizontal flow channels and stacked void or plenum spaces. It is believed, however, that this limitation has little effect on the predicted behavior of the plant during the transients discussed in this report.

The bottom reflector is divided into 2 zones (13 and 14). The lower or exit plenum is designated Zone 15. The graphite block in the

lower vessel region is Zone 16. Finally, the core support plate is designated as Zone 17, and, as is the case with upper support plate, is treated as an adiabatic boundary.

3.2 KONVEK Model

Figure 3.2 is a simplified schematic representation of the KONVEK model. This model employs 11 zones, most of whose boundaries physically coincide with those of the THERMIX model. Zone 1, which represents the inlet region of the coolant channels through the side reflector, serves as the "inlet plenum" for the helium coolant. Zone 2 is a "vertical

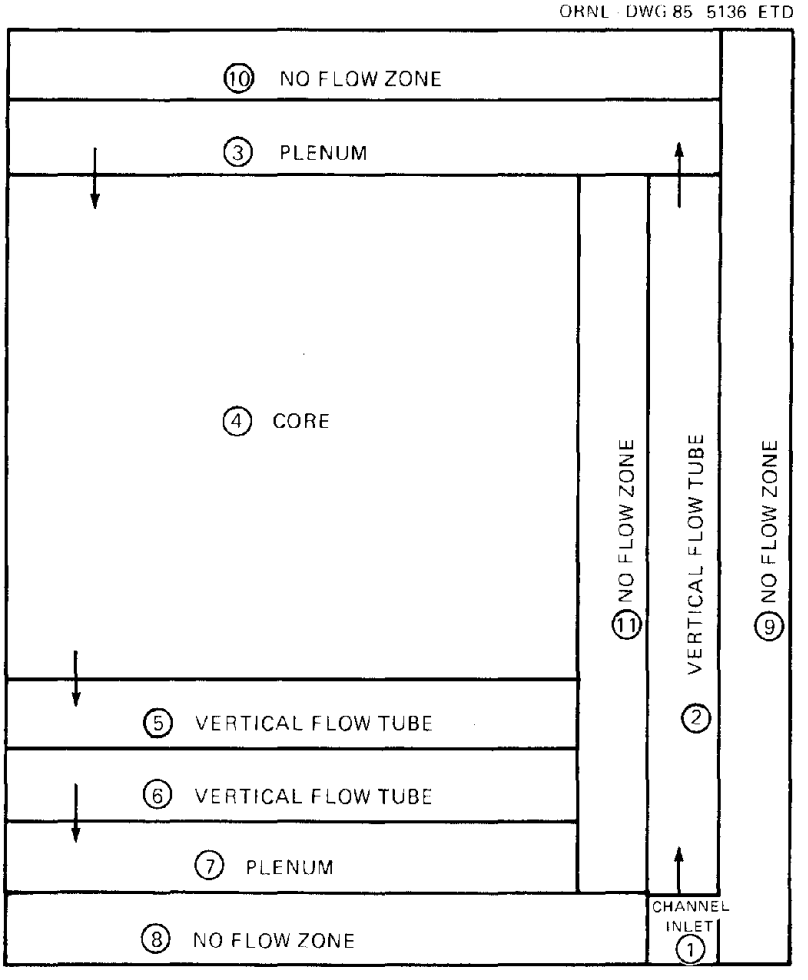

Fig. 3.3. Schematic representation of ORNL KONVEK model of U.S. pebble bed side-by-side modular HTR.

flow tube" zone which coincides with the middle side reflector zone of the THERMIX model and contains vertical channels in the graphite through which cold gas flows upward to the upper plenum. Zone 3 is the upper plenum which corresponds to Zone 9 of the THERMIX model. Zone 4 is the core zone, while Zones 5 and 6 represent the inner and outer sections of the bottom reflector; both Zones 5 and 6 contain vertical flow channels. Zone 7 is the lower (hot) gas plenum and, within the context of KONVEK, represents the mass sink for the system.

Within the KONVEK flow topology, helium enters the loop at Zone 1, flows up through the coolant channels in the side reflector (Zone 2) into Zone 3 (upper plenum), where it reverses direction, flowing downward through the core (Zone 4), and the bottom reflector (Zones 5 and 6), and out through the lower plenum (Zone 7) to the steam generator (not modeled). Zones 8, 9, 10, and 11 are "no flow" zones, which physically represent the carbon brick of the lower vessel, the outer side reflector, the inner upper reflector, and the inner side reflector, respectively.

4. TRIAL CALCULATIONS

A complete THERMIX-KONVEK transient analysis involves two executions of the code. In the first, the user provides the code with the basic information necessary to describe the model, as well as initial guesses for structural temperatures and coolant temperatures and pressures. Given this information, the code calculates a steady state temperature, pressure, and flow distribution for the entire reactor. The detailed initial temperature distribution is then incorporated into the transient input data set and the transient is then executed.

The following sections describe the results of the steady state calculation, the pressurized loss of forced convection (LOFC) transient, and the depressurized loss of forced convection (DPLOFC) transient analyses.

4.1 Initial Full Power Steady State Analysis

For the purpose of this calculation, the reactor was assumed to be operating at full rated power, flow, and pressure (250 MW_t, 114 kg/sec, and 72 bars, respectively). The axial and radial core power density profiles (which are based on the German THERMIX sample problem input with appropriate modification for core height and total power) are shown in Figs. 4.1 and 4.2. As shown in Fig. 4.1, the axial profile peaks just above the core midplane. For the purposes of this preliminary analysis, no attempt was made to modify the radial power density profile to reflect the presence of the core buttresses. Also, for these analyses, the power density in the top and bottom reflectors was set to zero.

The results of the steady state run are shown in Figs. 4.3 and 4.4. Figure 4.3 shows the predicted temperatures of the surface and center of the fuel elements and the coolant temperature as functions of core height (values displayed are those for the core center line). The maximum predicted fuel element center temperature is 782°C (axial core centerline at core outlet). In general, the coolant temperature is 20 to 30°C cooler than the fuel element surface temperature, while the fuel element center temperature is higher than the fuel surface temperature

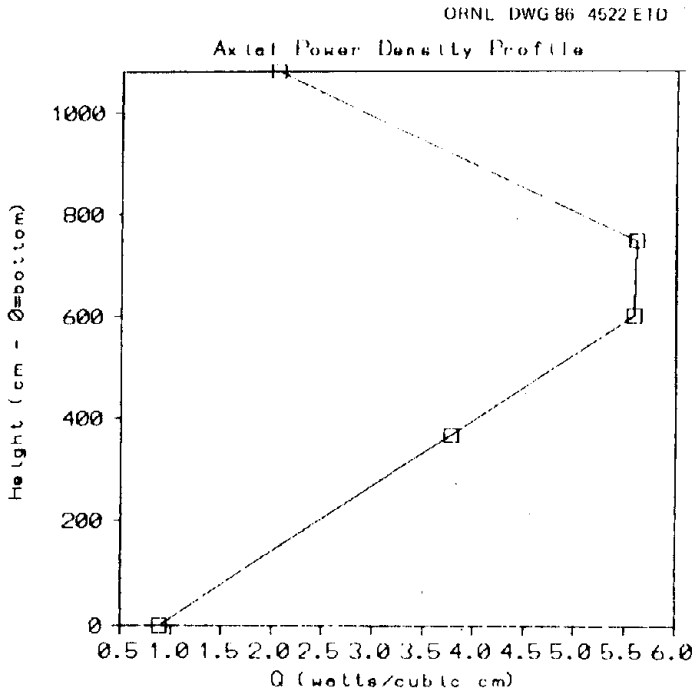

Fig. 4.1. Axial power density profile (axial centerline).

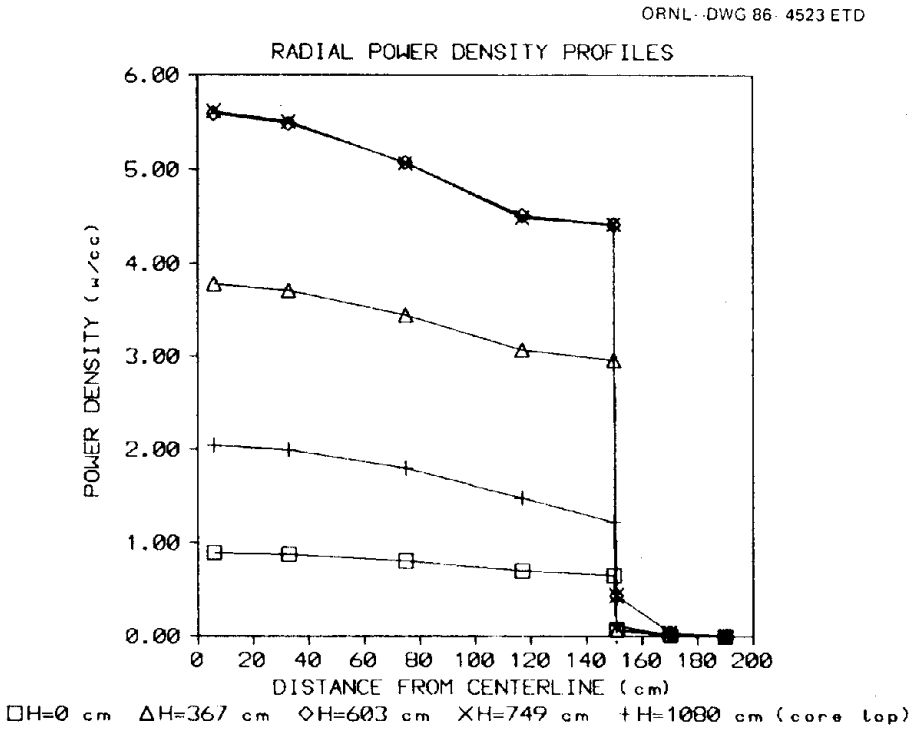

Fig. 4.2 Radial power density profile.

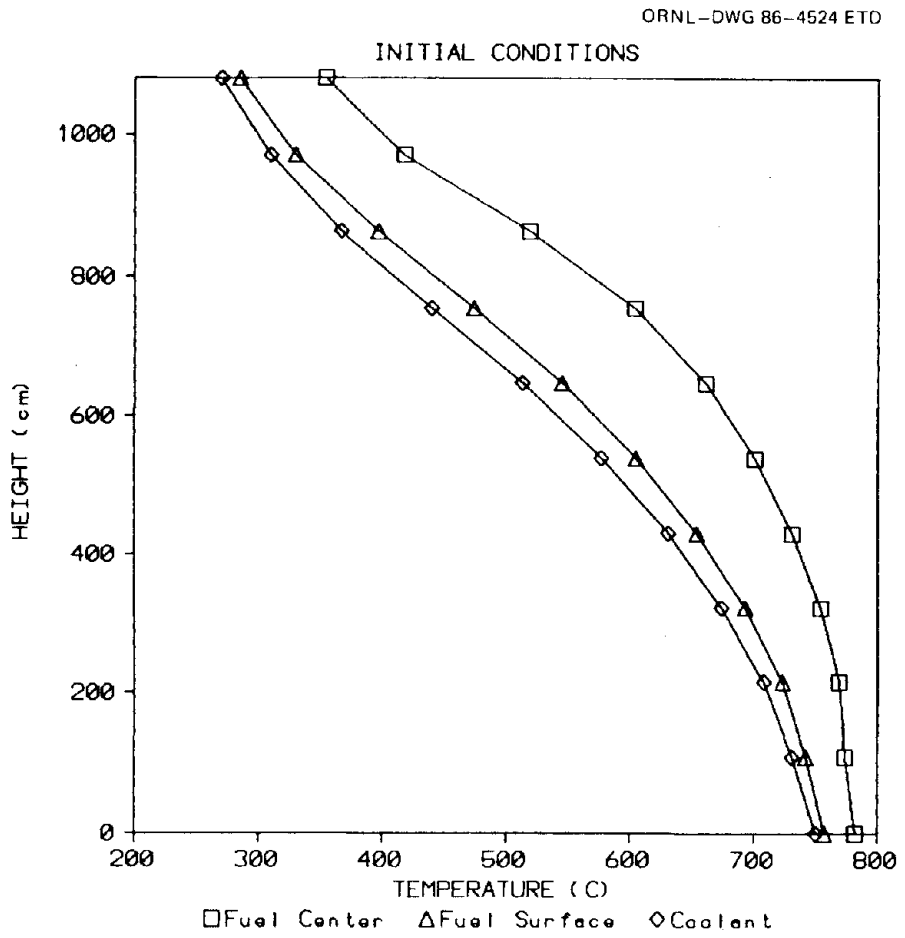

Fig. 4.3. THERMIX steady state case results: axial core temperature profiles (at core centerline).

by 60 to 120°C. As expected, the maximum fuel element temperature differences (center-to-surface) occur in the region from 600 to 800 cm above the core bottom, which (as shown in Fig. 4.1) is the region having the highest power density. The latter behavior is more clearly shown by Fig. 4.4, which shows the predicted steady state fuel element internal temperature distribution (as predicted by THERMIX) at three locations along the core centerline — at the top of the core, the core midplane, and the core outlet.

The steady state THERMIX case utilized 5-1/4 minutes of CPU time on the ORNL IBM 3033 system, with an associated cost of approximately $3 when executed under the "WHENEVER" option (executes only on weekends at a cost of about 10% of the prime time cost).

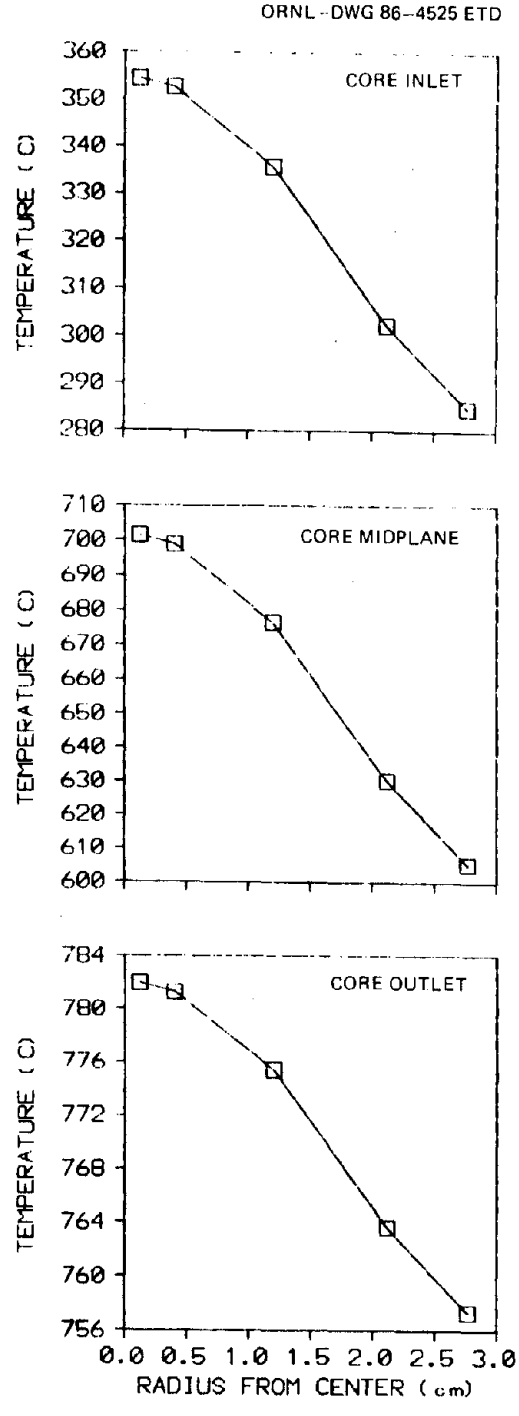

Fig. 4.4. THERMIX steady state case results: fuel element radial temperature profiles.

4.2 THERMIX Transient Results: Loss of Forced Convection and Loss of Main Heat Sink

The transient discussed in this section is an extreme example of the loss of forced convection (LOFC) transient, in which it is assumed that all forced flow into the reactor is instantaneously and permanently lost (i.e., there is no circulator coastdown), coincident with reactor scram. It is assumed that the reactor cavity cooling system continues to operate maintaining the reactor cavity wall temperature at 50°C. The THERMIX results for the first 44 h following initiation of the transient are shown in Figs. 4.5 through 4.8.

Figure 4.5 shows the maximum fuel temperature (regardless of location) as a function of time during the transient. Following initiation

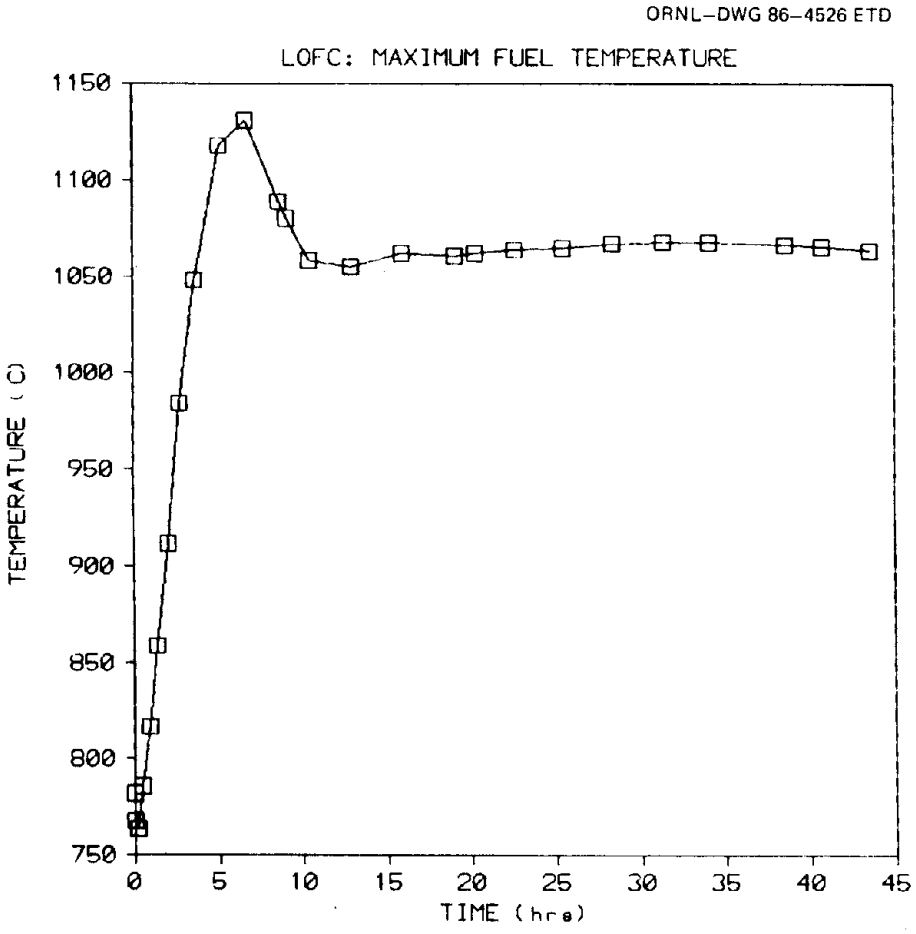

Fig. 4.5. THERMIX LOFC case results: maximum fuel temperature.

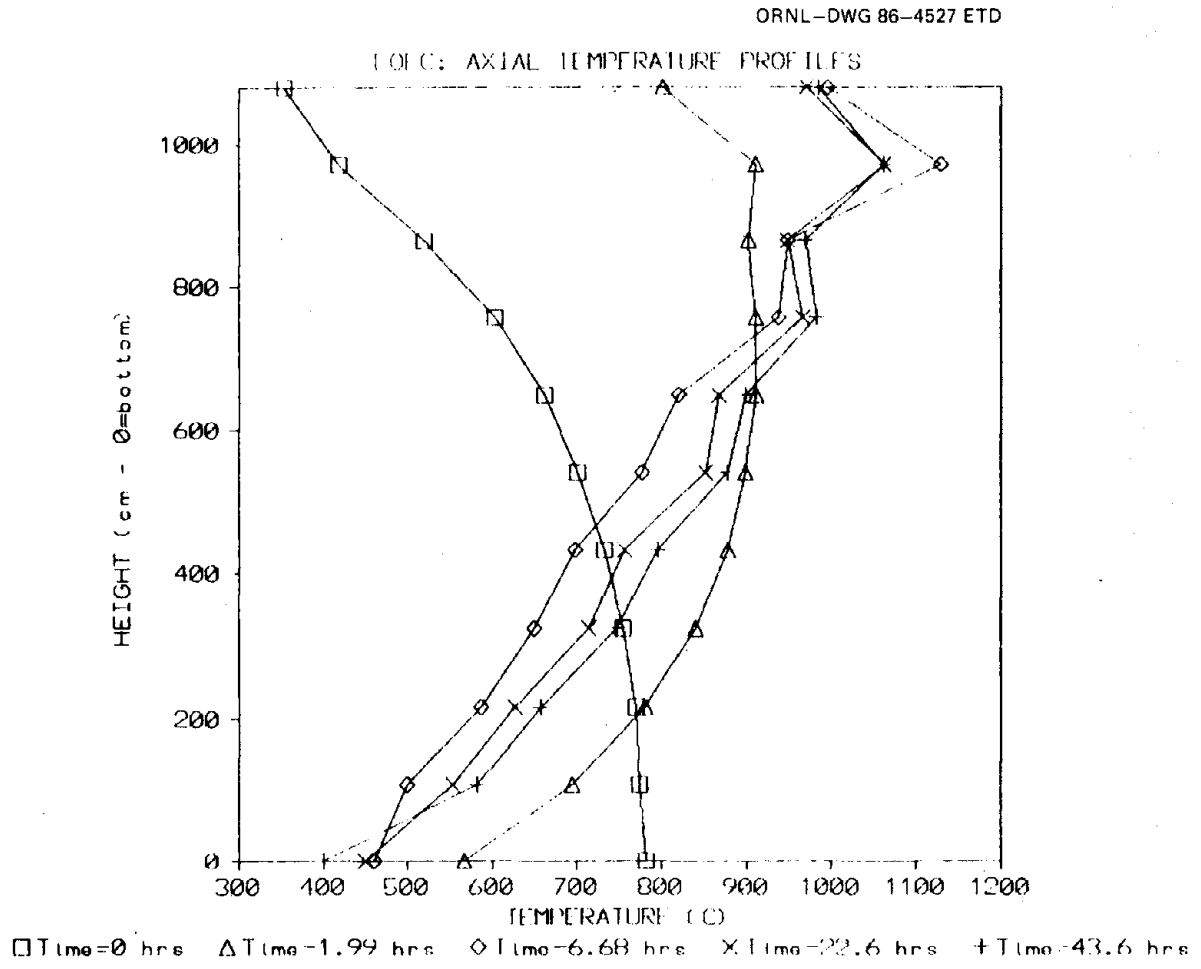

Fig. 4.6. THERMIX LOFC case results: axial fuel temperature profiles (at core centerline).

of the transient, the fuel temperature initially increases at a rate of about 65°C per hour and reaches a peak of 1131°C approximately 6.7 h into the accident. The location of the peak temperature is on the core center line, approximately 108 cm below the top of the core. Following this peak, the maximum fuel temperature begins declining, falling to a rather stable value of 1060°C, at approximately 10 h into the transient.

Axial core temperature profiles for five different transient times are shown in Fig. 4.6. This figure clearly shows the shift in the location of the maximum fuel temperature from the core outlet to the top of the core. This rather dramatic shift is due to the robust intra-core natural circulation which is established in the high pressure (~72 bar)

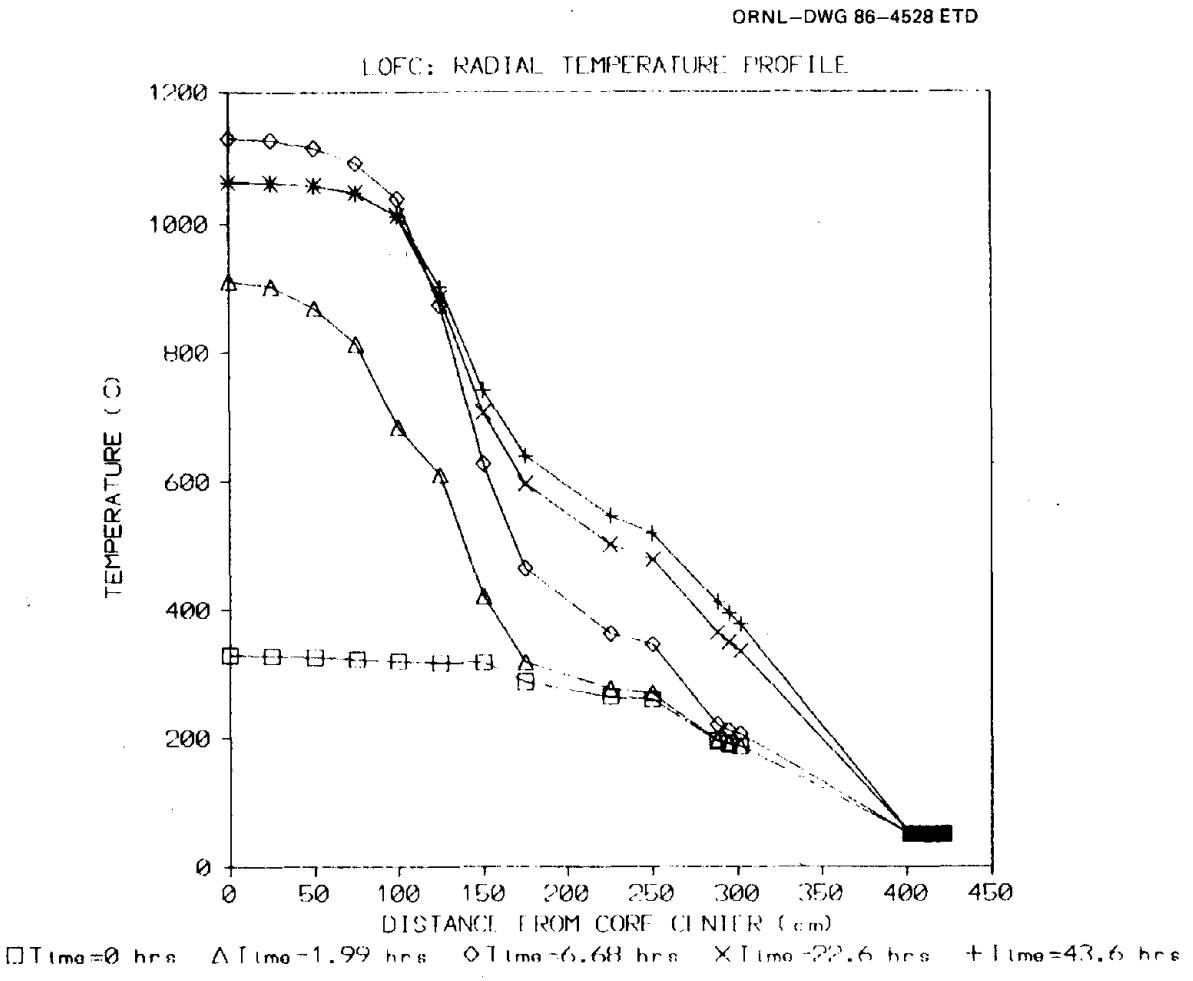

Fig. 4.7. THERMIX LOFC case results: reactor radial temperature profiles (at 108 cm below top of core).

environment. Although not depicted in the figures, THERMIX indicates that a natural convection cell is established in which hot helium rises through the inner 125 cm of the core and falls through the outer 25 cm of the core, along the cooler radial reflector wall. Typical values for the downward flow at core midplane in the outer 25 cm of the core are 0.3 to 0.45 kg/sec.

Figure 4.7 depicts the predicted radial temperatures profiles for the region 108 cm below the top of the core at five different times during the transient. It is apparent that the original flattened temperature profile is converted to a highly peaked profile during the first two hours of the transient. In particular, it is seen that the radial

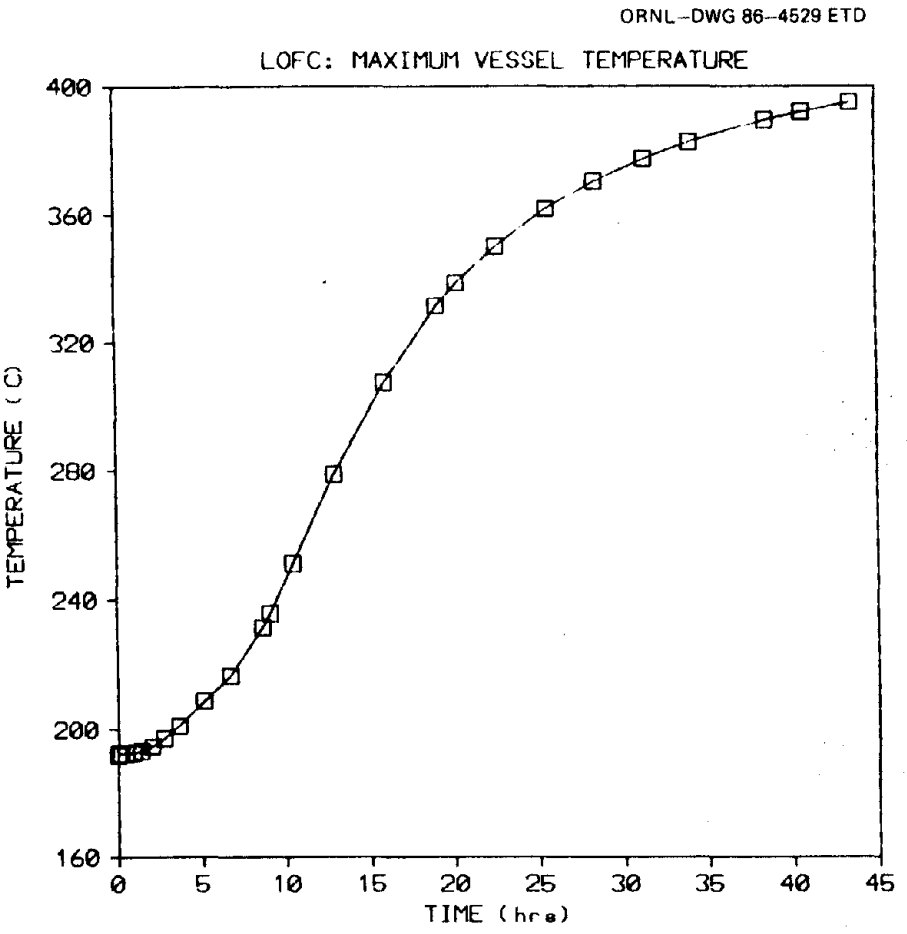

Fig. 4.8. THERMIX LOFC case results: maximum reactor vessel temperature.

reflector temperature (the region between 150 and 250 cm) is several hundred degrees cooler than the inner regions of the core for the first several hours of the transient. This temperature difference is reduced at later times, however, due to heat transport from the inner radial zones to the outer zones of the reactor.

Conductive, radiative, and convective heat transport mechanisms result in a gradual increase in the temperature of the reactor vessel wall. Figure 4.8 is a plot of the maximum reactor vessel wall temperature during the first 44 h of the transient. The temperature is seen to increase from an initial value of 192°C at the beginning of the transient to 395°C at 44 h into the accident. It should also be noted that the vessel temperature is still increasing at the end of the analysis period. Further investigations should, therefore, be conducted to

determine the maximum temperature in the vessel wall during this transient, and whether such temperatures pose any threat of reactor vessel damage.

4.3 THERMIX Transient Results: Depressurized Core Heatup with Loss of Forced Convection

The reactor transient discussed in this section is a depressurized version of the LOFC accident discussed in Sect. 4.2. In particular, the reactor is assumed to scram coincidentally with an instantaneous loss of all forced flow and an instantaneous depressurization from 72 bars to 1 bar. Again it is assumed that the reactor cavity cooling system continues to operate maintaining the cavity wall temperature at 50°C. The results of the THERMIX analysis of this accident are depicted in Figs. 4.9 through 4.12.

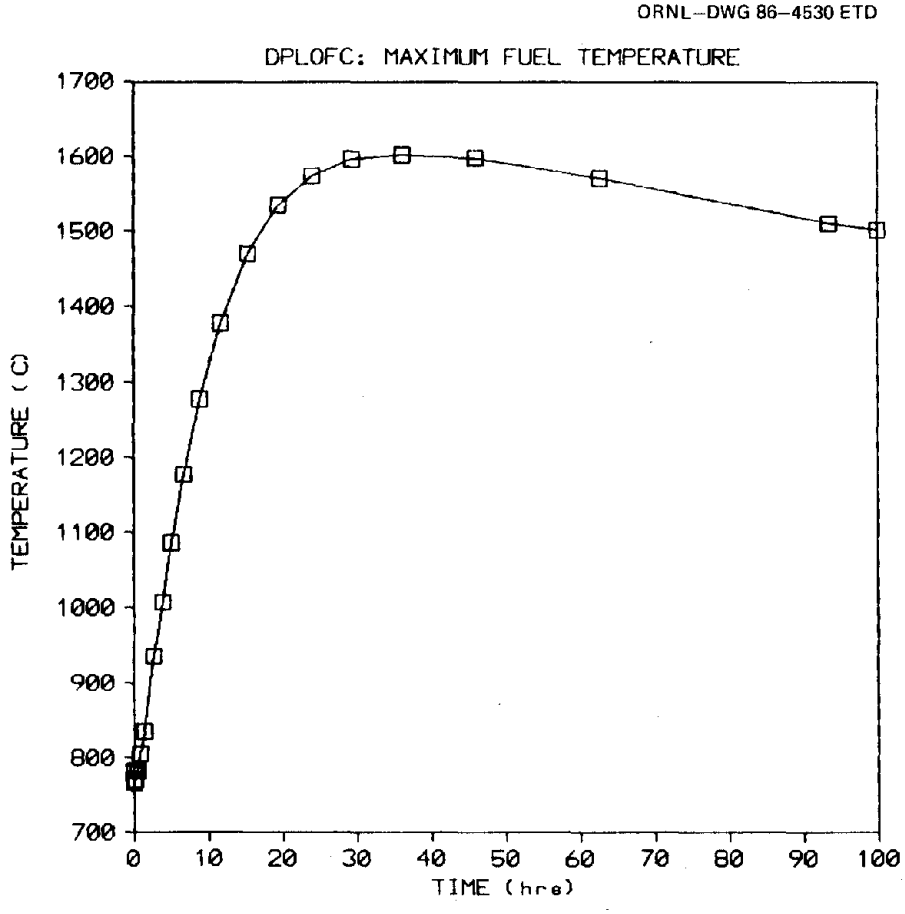

Fig. 4.9. THERMIX depressurized LOFC case results: maximum fuel temperature.

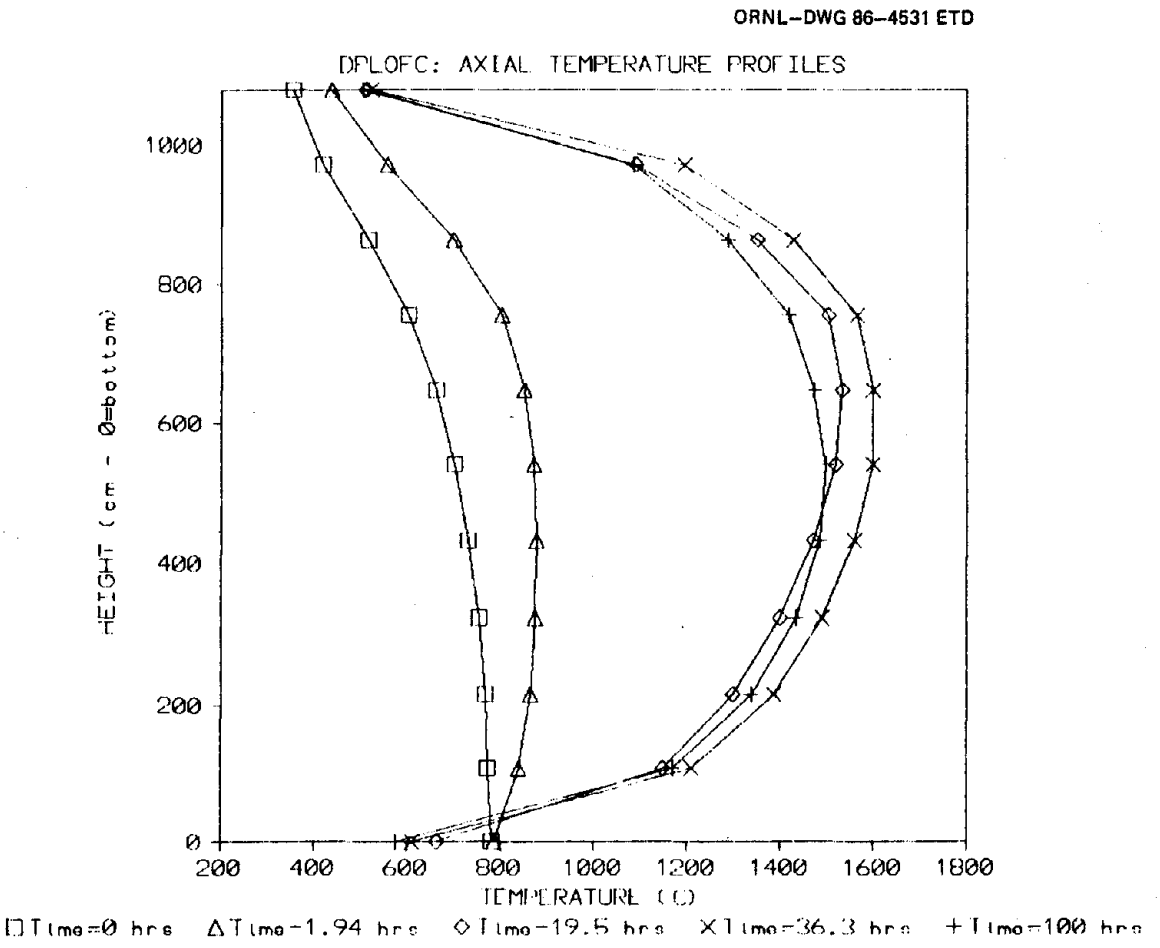

Fig. 4.10. THERMIX depressurized LOFC case results: axial fuel temperature profiles (at core centerline).

Figure 4.9 is a plot of the maximum fuel temperature as a function of time during the transient. Following accident initiation, the maximum fuel temperature initially increases at the rate of approximately 50°C per hour, and reaches its maximum value of 1603°C at 36.3 h into the transient. [Note that the initial rate of temperature increase for the pressurized LOFC was actually higher than for this depressurized case. For the pressurized LOFC case this behavior is due to convection of hot gas from the lower to the upper region of the core during the early phase (first 2 to 3 h) of the transient. The fuel elements in the upper core zones, which eventually become the hottest elements, are actually heated by the hot gas during this period.]

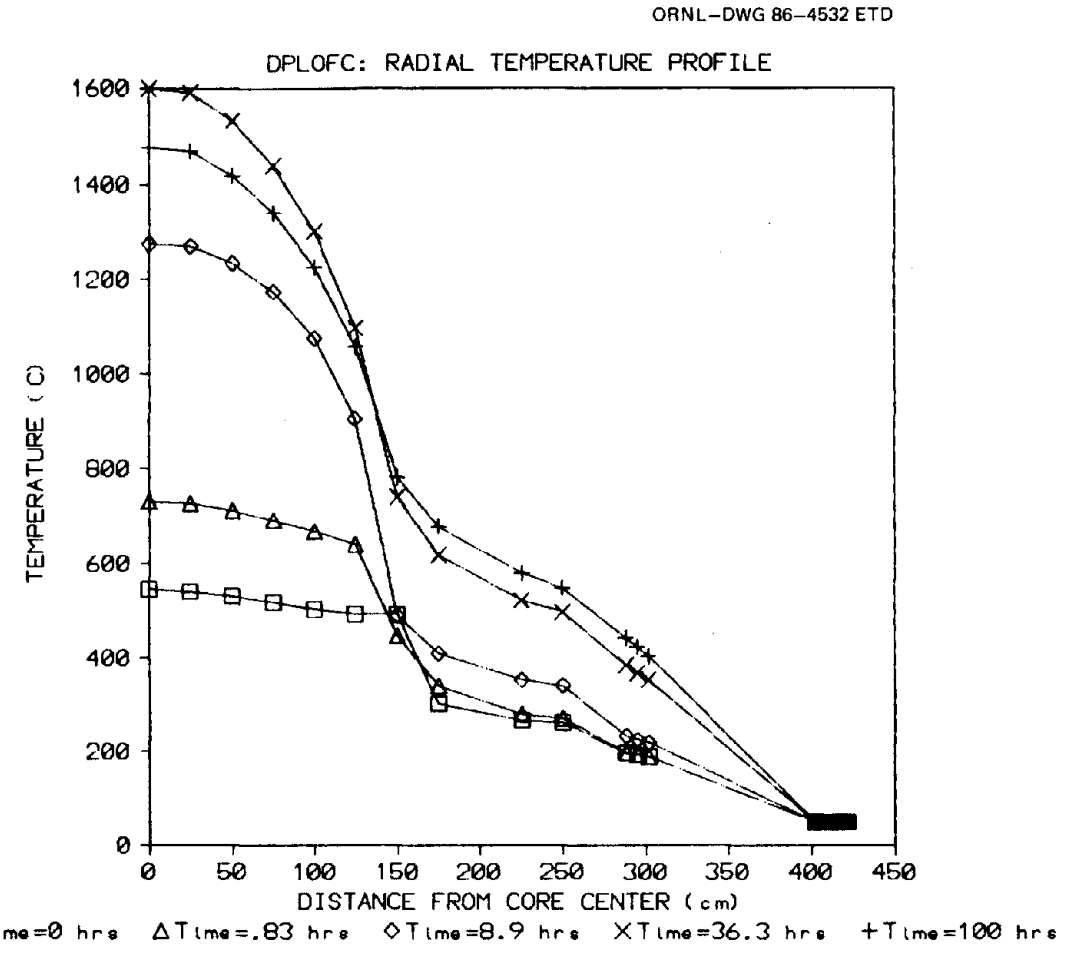

Fig. 4.11. THERMIX depressurized LOFC case results: radial reactor temperature profiles (at 432 cm below top of core).

As depicted in Fig. 4.10, this maximum fuel temperature occurs at a point 432 cm below the top of the core (i.e., approximately 1 m above the core midplane). The maximum fuel temperature remains near 1600°C for approximately 10 h, but only 8 of the 77 THERMIX core nodes ever exceed 1550°C. The maximum fuel temperature begins to slowly decline after 46 h, reaching a value of 1502°C at 100 h into the accident.

Figure 4.11 depicts the radial temperature profiles at five distinct times during the accident (profiles depicted are for the zone 432 cm below the top of the core). The smoothness of the plots can be attributed to the large heat capacity of the HTR core and good intercell heat transfer. The large core heat capacity is also responsible for the rather large time lag (approximately 9 h) between transient

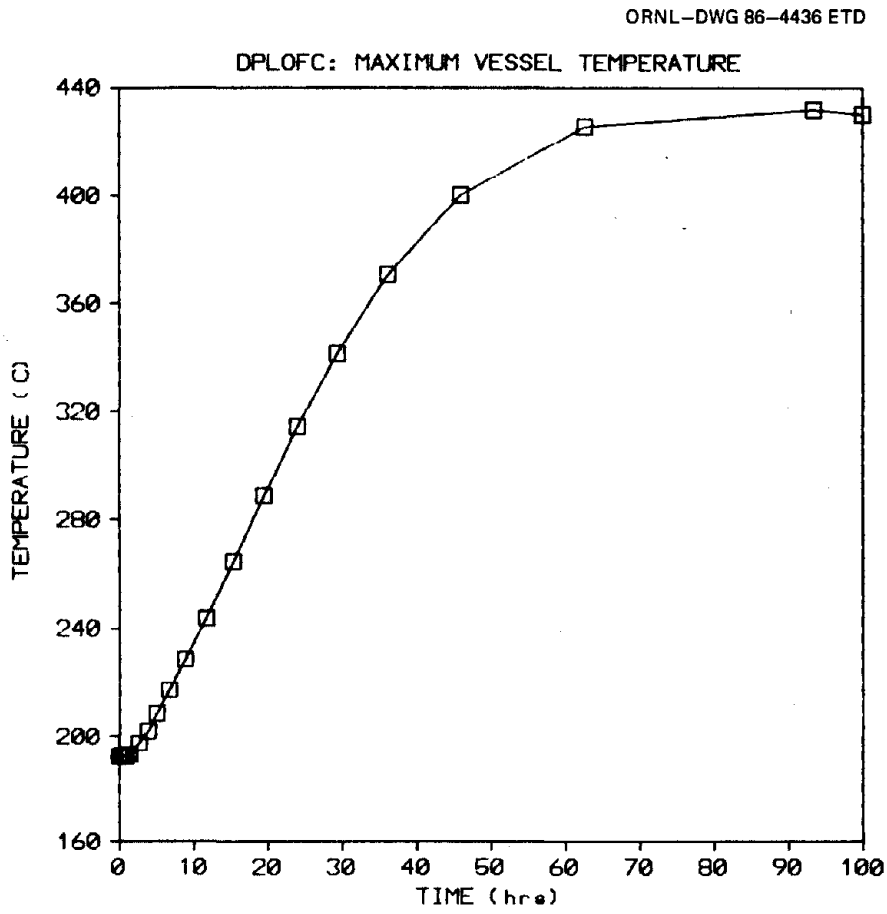

Fig. 4.12. THERMIX depressurized LOFC case results: maximum reactor vessel temperature.

initiation and the occurrence of any significant increases in the temperature of the radial reflectors (the region between 150 and 250 cm).

Figure 4.12 displays the maximum reactor vessel temperature as a function of time during the transient. Following initiation of the accident, the vessel temperature rises at the rate of approximately 7°C per hour, reaching its maximum temperature of 432°C at 93.5 h into the transient. The plot also indicates that the temperature of the reactor vessel begins to decrease by 100 h into the transient.

The depressurized LOFC THERMIX case utilized 20 min of CPU time on the ORNL IBM 3033 system, with an associated cost of approximately $11 when executed under the "WHENEVER" option.

4.4 Comparisons with Results of Other Analyses of Modular Pebble Bed HTRs

The design goals for the U.S. 250 MW(t) modular (side-by-side) pebble bed HTR are such that the maximum fuel temperatures remain below 1600°C during depressurized core heatup accidents and below 1200°C for pressurized loss of forced circulation, LOFC, including loss of main heat sink, events. As noted in Sects. 4.2 and 4.3, the ORNL's analyses predict a maximum fuel temperature of 1603°C under depressurized core heatup conditions and a maximum fuel temperature of 1131°C under pressurized LOFC including loss of main heat sink conditions.

These results can also be compared with predictions for the same accident conditions for Interatom's 200 MW(t) modular (side-by-side) pebble bed HTR. This concept is quite similar to the U.S. modular pebble bed HTR. For example, core diameter, which is an important parameter in determining maximum fuel temperature, is the same as for the U.S. design. The Interatom design has a lower total power [200 MW(t)], a lower core power density (3.0 W/cm^3), a slightly reduced core height (9.4 m), and operates at somewhat lower pressure (60 bar). The Interatom concept is modeled by the THERMIX-KONVEK sample problems (a steady state case and a depressurized core heatup case) provided by KFA to ORNL. (As noted in Sect. 3, KFA considers the representation of Interatom's design as provided in the sample problem to be preliminary and not completely accurate.) For the depressurized core heatup, the sample problem predicted a maximum temperature of 1520°C. This problem was then re-run with a higher initial power density and core flow rate corresponding to 250 MW(t). With this initial power level, a maximum fuel temperature of 1690°C was reached in a depressurized core heatup case. (This is to be compared with the prediction of 1603°C for the U.S. 250 MW(t) side-by-side modular pebble bed HTR. The somewhat lower temperature for the U.S. design is due to the slightly taller core and hence lower maximum power density.)

A pressurized LOFC with loss of main heat sink case was also run using the model for the Interatom 200 MW(t) concept. This resulted in a maximum fuel temperature of 1055°C which is about 75°C lower than that

predicted by ORNL's analysis of the U.S. 250 MW(t) concept for this accident. This is due to the lower core power of the Interatom concept.

The above THERMIX results can also be compared with earlier ORNL results (Ref. 8) for a vertical-in-line 250 MW(t) pebble bed modular HTR. The ORNL result for peak fuel temperature during a depressurized loss of forced circulation accident for the vertical-in-line design is 1549°C. Given the somewhat different core dimensions, power density, and power distribution for the vertical-in-line concept, this is not significantly different from the 1603°C value obtained in the THERMIX analyses of the side-by-side pebble bed modular HTR. For the vertical-in-line concept in the event of a pressurized LOFC including loss of feedwater flow to the steam generator, ORNL predicts a peak fuel temperature of 910°C. This is lower than the 1131°C THERMIX prediction for the side-by-side concept primarily because of the significantly larger natural circulation flows which are established with the vertical-in-line concept. While loss of feedwater can be made to be highly unlikely by incorporation of an auxiliary feedwater system, with the vertical in-line design it could result in damage to the steam generator since the hottest steam generator tubes would approach temperatures of approximately 800°C.

5. THERMIX-KONVEK VALIDATION

5.1 Summary of THERMIX-KONVEK Validation

This section summarizes KFA's validation efforts for THERMIX-KONVEK as well as their efforts to determine appropriate correlations for representing the effective conductivity of the pebble bed. These efforts are obviously coupled because the agreement of THERMIX-KONVEK predictions with experimental data depends in part on the appropriateness of the representation of the bed conductivity.

5.1.1 Investigations of effective conductivity in a pebble bed without gas flow

As is discussed in Sect. 2, the total thermal conductivity of the bed consists of the effective conductivity (λ_e in Eq. 1) independent of coolant flow including pebble-to-pebble conduction, radiation and conduction within pebbles, and the dispersive thermal conductivity of the gas (λ^* in Eq. 5). This section summarizes investigations of λ_e. A summary of investigations of dispersive heat transport is included in Sect. 5.1.3.

In examining various correlations for λ_e (the effective bed conductivity independent of coolant flow), several factors must be kept in mind. This effective conductivity is dependent (at least) on local temperature, pebble diameter, pebble emittance, local void fraction, pebble internal conductivity (matrix conductivity), fluid conductivity, and a local contact parameter (dependent on surface roughness and contact pressure of the pebbles). Thus

$$\lambda_e = \lambda_e(T,\ d,\ e,\ \varepsilon,\ k,\ \lambda_{gas},\ s)\ .$$

Also, it may be dependent on local temperature gradient. λ_e increases with increasing temperature, emissivity, pebble conductivity, and the contact parameter. λ_e decreases with increasing void fraction.

The correlation used in THERMIX (see Eq. 6, Sect. 2.2.2 of this report) is a simplification for at least the following reasons:

1. The correlation is a function of temperature only.

2. A constant matrix graphite conductivity, k, is built in to the correlation. In fact, matrix graphite conductivity is itself a function of irradiation temperature, fluence, and current temperature: i.e.,

$$k_{matrix} = k_{matrix}\ (T_{irrad},\ fluence,\ T)\ .$$

3. The correlation assumes a void fraction of 0.39 and is applied over the entire bed. In fact the void fraction varies considerably near the bed boundary (see Fig. 5.1). The dependence of void fraction on distance from the wall is carefully examined in Ref. 9. As can be seen, the statistically mean void fraction of 0.39 is established after about five pebble diameters. High void fraction reduces the effective conductivity as presented in Ref. 10 and discussed later in this section.

In Ref. 11, Breitbach and Barthels discuss theoretical models and experimental results for the effective thermal conductivity for a bed of spheres in a vacuum. In their paper, theoretical models developed by Zehner and Schluender and by Vortmeyer for applications to packed beds in the chemical industry are applied to pebble bed conditions. Also, Breitbach and Barthels describe experiments performed at KFA using the High Temperature Vacuum Oven (see Fig. 5.2). In these experiments a

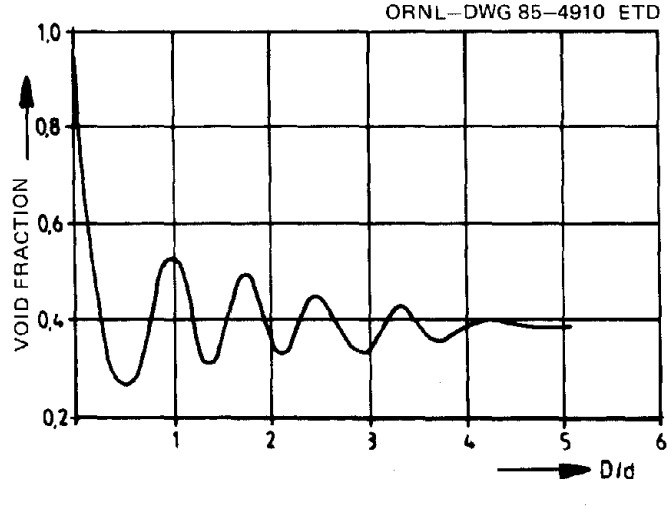

Fig. 5.1. Variation in void fraction near bed boundary. (Figure taken from Ref. 9.)

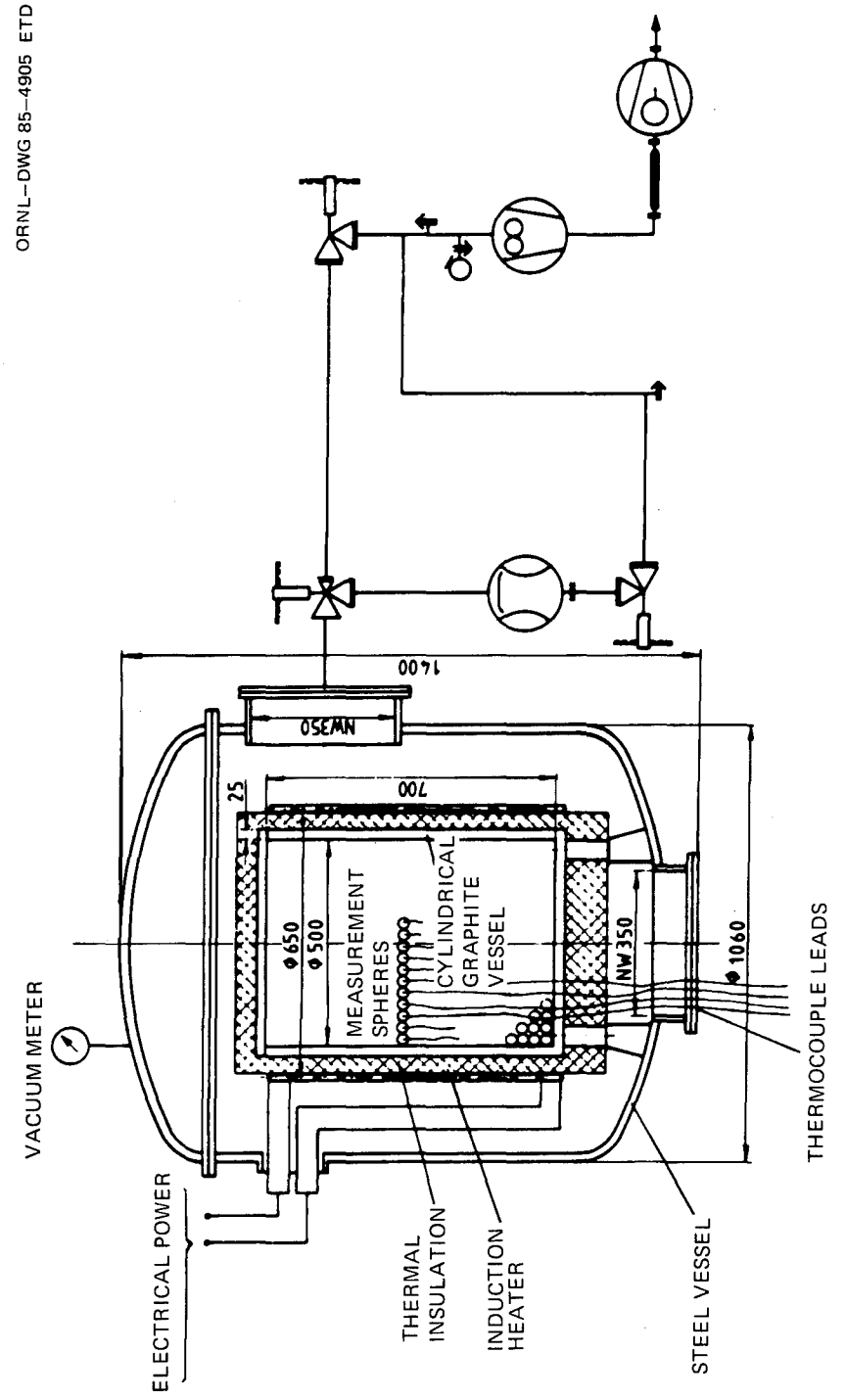

Fig. 5.2. High temperature vacuum oven facility of KFA. (Figure taken from Ref. 10.)

transient measurement method was used to determine the effective thermal conductivity in beds of Zirconium oxide pebbles (4.5 cm diam) and in beds of (unirradiated) graphite pebbles (4.0 cm diam) at temperatures up to 1000°C and 1500°C, respectively. (ZrO_2, which has an emittance of 0.4 at 725°C, was used to test the theoretical models because the two models give markedly different predictions of effective conductivity for pebble beds of materials with low emittance.) Comparison of measured results with the theoretical model of Zehner and Schluender and with the theoretical model of Vortmeyer showed discrepancies which led Breitbach and Barthels to suggest corrections to both models. Breitbach and Barthels used the corrected models to predict values of λ_e for pebble bed HTRs (6 cm diam pebbles, void fraction = 0.40 and pebble emissivity = 0.8), with k_{matrix} = 15 W/mK (independent of temperature) and for temperatures ranging from 1000 to 2750°C. These predictions are shown in Fig. 5.3.

A more recent review by Schürenkrämer (Ref. 3) of theoretical models and experimental results for effective conductivity for a bed of

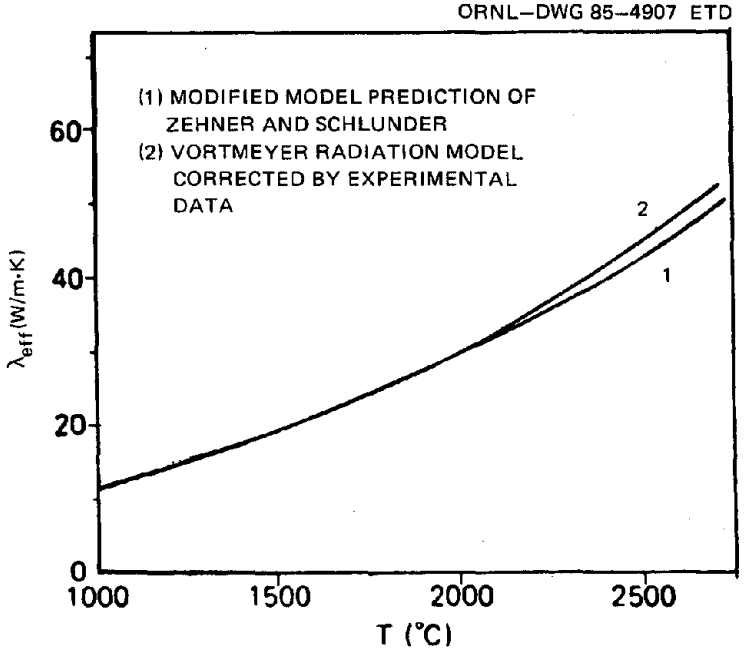

Fig. 5.3. Effective conductivity of a packed bed of graphite pebbles. (Figure taken from Ref. 11.)

1.905 cm diam steel spheres (up to 300°C) resulted in a modified representation for effective conductivity of a bed of 6 cm diam graphite pebbles:

$$\lambda_e = 2.549 \times 10^{-4}\ T^{1.545} + 1.5 \text{ for } T < 1300°C\ ,$$

and

$$\lambda_e = 2.0 \times 10^{-3}\ (T - 135)^{1.287} \text{ for } T \geq 1300°C\ ,$$

with λ_e in W/mK and T in °C. (The value of k_{matrix} on which this correlation by Schürenkrämer is based is for NUKEM A3-4 graphite irradiated at 850°C to a fast fluence of 4×10^{21} EDN/cm^2.)

The effect of the increased void fraction on λ_e near the reflector wall of a pebble bed reactor is shown in Fig. 5.4 (taken from Ref. 10).

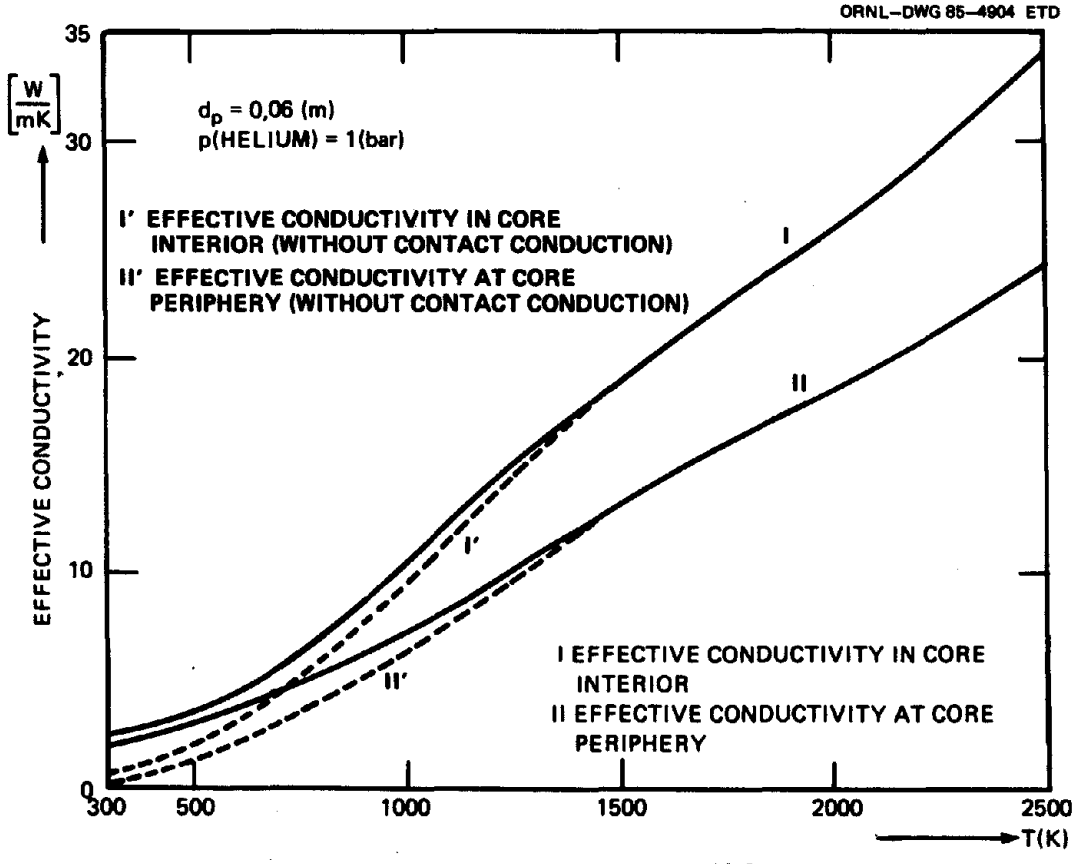

Fig. 5.4. Effective conductivity in the interior and at the periphery of a pebble bed core. (Figure taken from Ref. 10.)

In Ref. 10, Robold presents the variation in λ_e (at 1 bar pressure) in the inner region of the pebble bed (6 cm diam graphite pebbles, $\varepsilon = 0.39$) compared to the region near the reflector. Curve I in Fig. 5.4 shows λ_e for the inner zone of the pebble bed and curve II shows λ_e in the region

$$0 < x < 0.5\ d_{pebble}$$

near the reflector wall.

Curves I′ and II′ show Robold's results with the assumption that there is no contact heat conduction. In deriving the curves shown in Fig. 5.4, Robold used values for matrix graphite thermal conductivity and for graphite emissivity shown in Table 1. In comparison with thermal conductivity values for matrix graphite at various fluence levels presented in Ref. 12, the values in Table 1 appear to have been selected for unirradiated NUKEM A3-3 graphite. This would tend to result in higher-than-expected values for λ_e for an actual pebble bed with irradiated fuel.

Table 1. Graphite material properties used in deriving effective conductivities shown in Figure 5.4

(Table values excerpted from Ref. 10)

T(K)	300	500	700	900	1100	1300	1500	1700	1900	>1900
k(W/mK)	52.0	40.5	33.7	29.2	26.0	23.3	21.2	19.2	17.3	15.0
ε	0.7	0.78	0.85	0.88	0.88	0.90	0.89	0.89	0.88	0.88

5.1.2 Experimental validation of THERMIX-KONVEK using the KFA Small Research Rig

The first experimental tests of the THERMIX-KONVEK program were conducted at KFA in the Institute for Reactor Components during 1975—1976 in the Small Research Rig. A schematic of this facility is

shown in Fig. 5.5. The facility included

- A pebble bed (40 cm high by 24.8 cm diam) consisting of steatite spheres (1 cm diam) was contained in a steel pressure vessel. The system could accommodate a gas pressure up to 40 bars.
- Above the surface of the pebble bed there was a void of 30 cm height. In a later series of experiments a top cooler (simulating, for example, an auxiliary heat removal system) was installed in the void.
- The steel pressure vessel was surrounded by a water circulating system in its jacket region by which the bed of steatite spheres could be initialized to a uniform temperature and allowing rapidly variable temperatures at the vessel wall. The vessel was insulated at top and bottom.

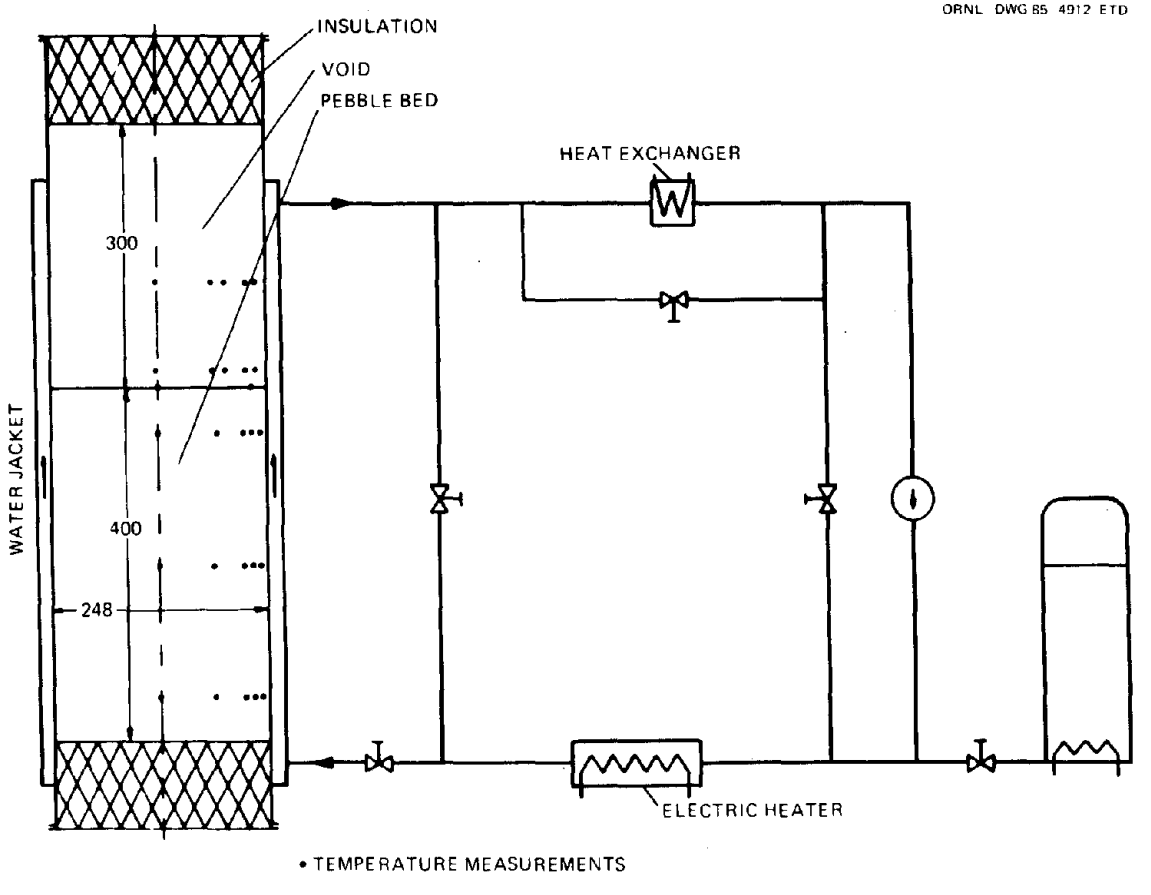

Fig. 5.5. Small research rig at KFA. (Figure taken from Ref. 13.)

- Special steatite spheres into which thermoelements were inserted were placed at 23 different axial, radial, and azimuthal positions to record time varying temperatures. Thermoelements were also placed in the void region above the bed, at the vessel wall, and in the water jacket system.

The goal of the tests (Ref. 1) was to examine heat transport within the bed of spheres by natural convection and by conduction and radiation. The effect of natural convection could largely be separated from that of conduction/radiation by adjusting system pressure and by changing the type of gas (options included air, N_2, and CO_2).

The various tests were typically conducted with the following procedure:

a) The system was charged with gas to a specified pressure.

b) The pebble bed was brought to a uniform temperature (either ambient or a higher level up to 100°C) by circulation of water through the water jacket.

c) The transient was initiated by introducing a rapid change in the temperature of the heating jacket, followed by maintenance of this temperature at the new level. Both heatup and cooldown transients in the bed were investigated.

d) The time dependent temperature profile in the bed and gas pressure were measured, and results compared with THERMIX-KONVEK predictions.

Results are reported in Ref. 13 and code predictions are in fair agreement with measured results. Figure 5.6 shows typical results for the heat transport experiments. This figure presents a comparison of calculated and measured results for temperatures on the vertical axis for experiments using N_2 at 1 and at 20 bars. In each experiment the initial temperature of the water jacket was at ambient and the experiment was initiated by rapidly changing the water jacket temperature to 100°C. At 1 bar, heat transport by conduction/radiation dominates, and at 20 bars, heat transport by convection dominates.

Figure 5.7 shows typical results for the time dependence of the temperatures in the periphery of the bed. The test shown was performed

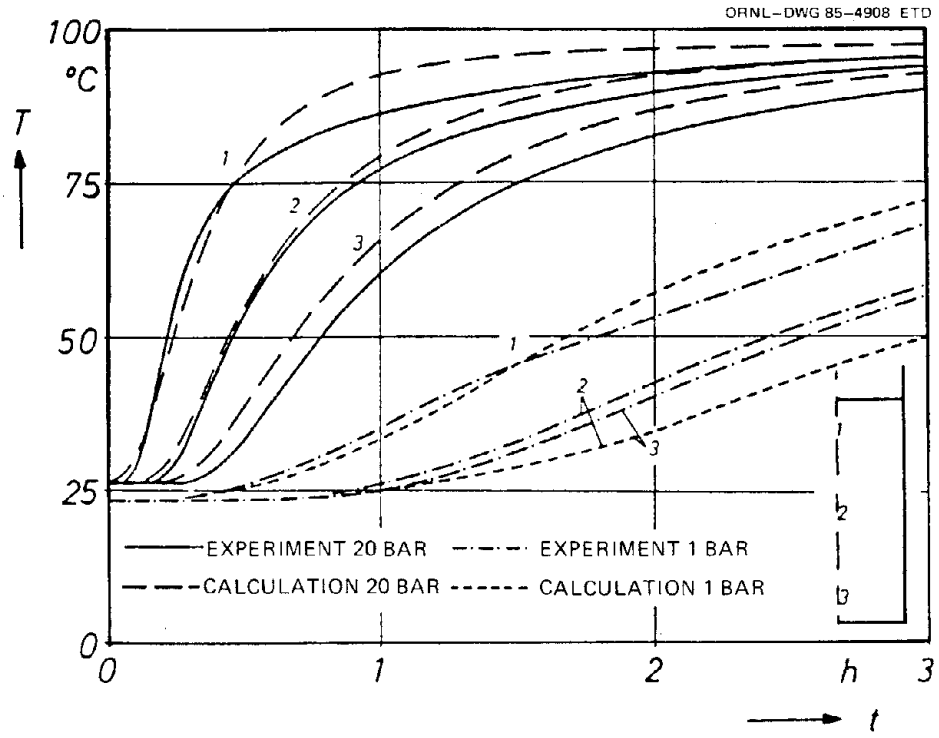

Fig. 5.6. Time dependent temperature profile along vertical axis in bed of steatite spheres during heatup test. (Figure taken from Ref. 13.)

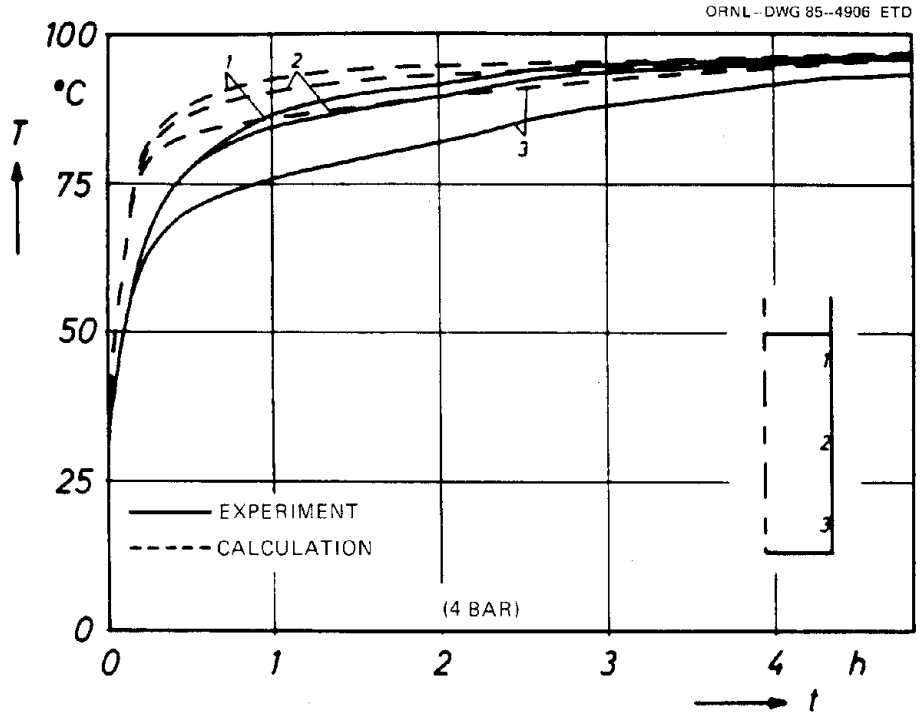

Fig. 5.7. Time dependent temperature profile near the boundary of a bed of steatite spheres during heatup test. (Figure taken from Ref. 13.)

with N_2 at 4 bars. For this condition, the components of the heat transport due to natural convection and due to conduction/radiation are approximately equal. Typically, the agreement between calculated and measured results was not as good in the peripheral region of the bed as it was along the axis of the bed.

Experiments in this facility formed the basis for planning the construction of the large research rig and the subsequent tests.

5.1.3 Experimental validation of THERMIX-KONVEK using the KFA Large Research Rig

A schematic of the Large Research Rig (also referred to as the high pressure test loop) at KFA's Institute for Reactor Components is shown in Figs. 5.8-a and 5.8-b. The facility includes

- A pebble bed (120 cm high by 70 cm diam) filled with steel pebbles (diam = 1.905 cm) contained in a 1 cm thick steel vessel. This steel vessel is enclosed by an external pressurizer steel shell which contains a water jacket. Between the internal vessel and the

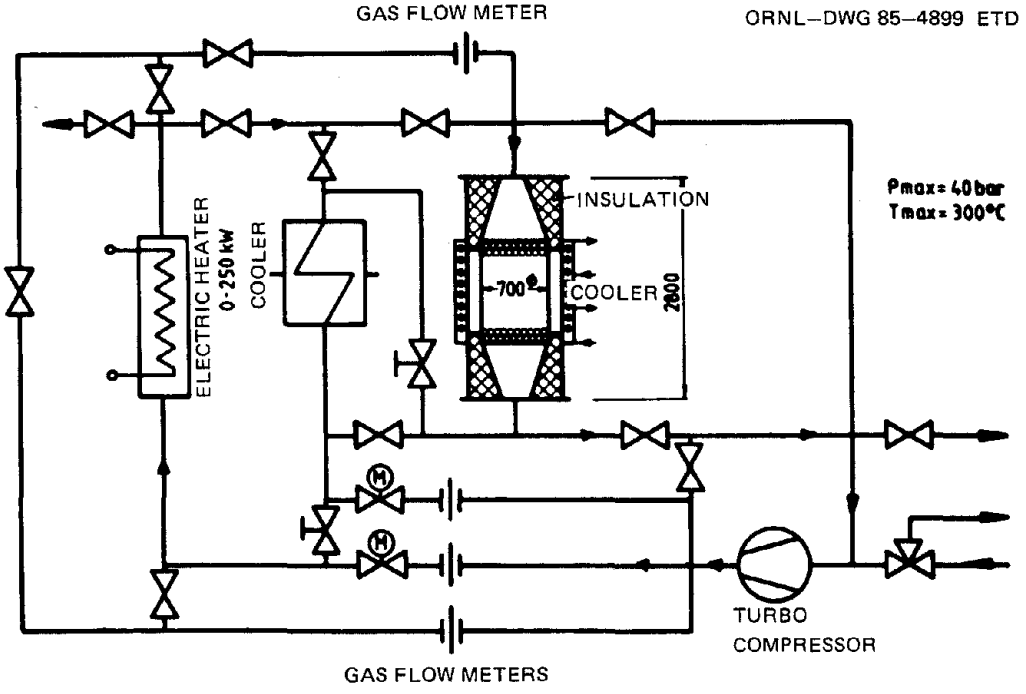

Fig. 5.8-a. Schematic of the large research rig at KFA. (Figure taken from Ref. 3.)

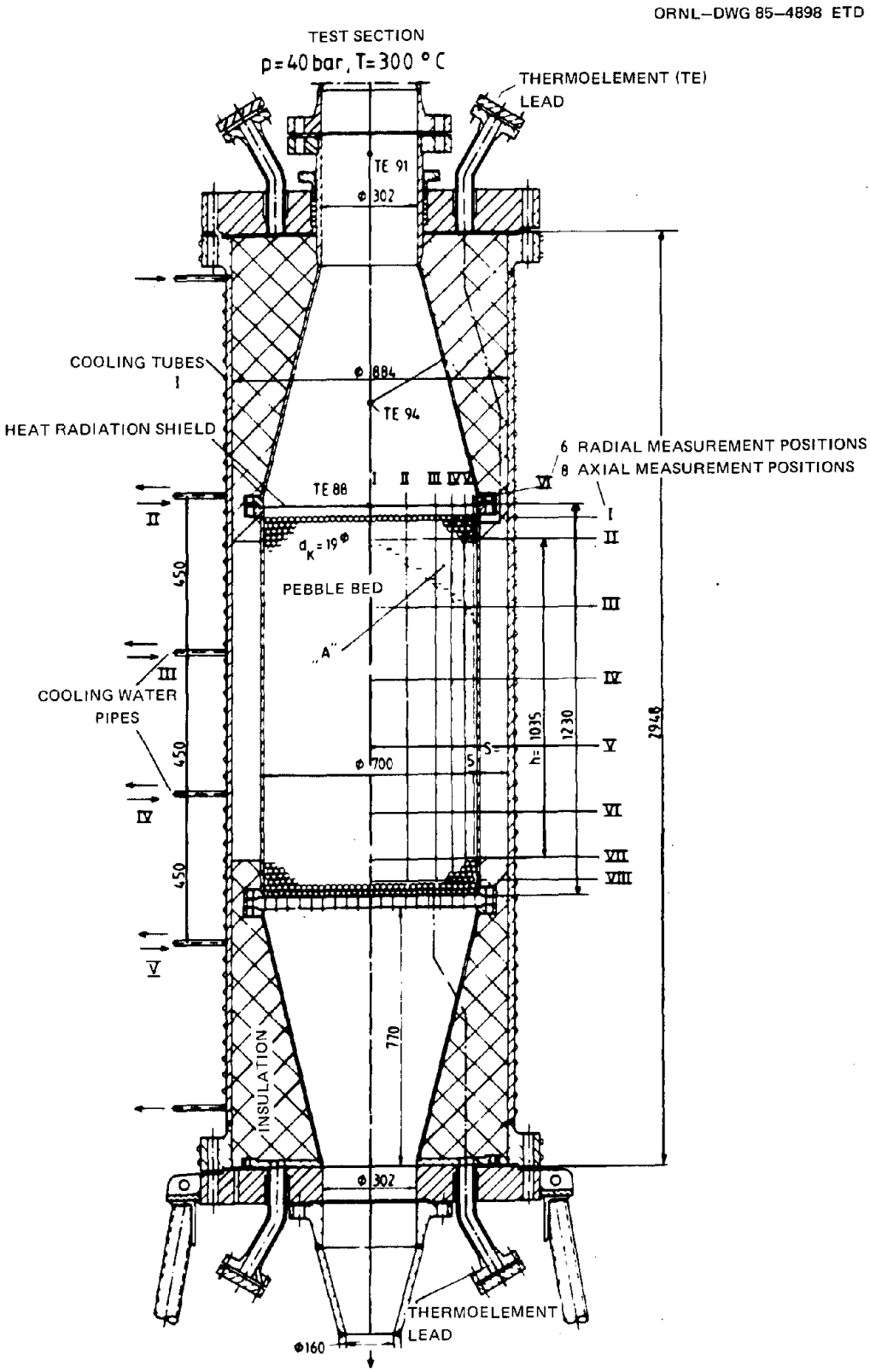

Fig. 5.8-b. Test section of the large research rig. (Figure taken from Ref. 3.)

pressure shell in the funnel region there is insulation for the purpose of avoiding heat losses so that cooling of the bed essentially occurs radially through the annular gap. The system can accommodate pressure up to 40 bars and temperatures up to 300°C by means of a compressor and an electric heater.

- Gas flow enters at the top flowing downward through the bed. Above the pebble bed is a void. In some tests a "point source" of gas could be injected at a position on the axis 30 cm below the bed surface.
- Special steel spheres containing thermoelements were placed at 79 selected locations in the bed to measure the time dependent temperature profile. Time dependent temperatures along the inner vessel wall and in the water jacket were also measured along with water flow rate. The measured temperatures on the inner vessel wall were input to THERMIX as boundary conditions. The forced helium flow was also measured.

The objective of the experiments was to investigate heat transport in the pebble bed by natural and forced convection and by conduction/radiation.

Results of experiments conducted on this loop are reported in Refs. 3 and 5. Typically, the experiments were conducted in the following manner:

- The bed was brought to a uniform temperature (300°C) by forced flow of hot gas (air or helium).
- The system pressure was adjusted to the desired level (1 to 30 bars).
- The gas circulator was turned off.
- The test section was isolated by closing valves at the inlet and outlet so that natural circulation was limited to the inner area of the test section.
- Water flow through the cooling tubes was adjusted to maintain the wall temperature at about 30°C.

The factors investigated included:

1) the extent to which a rotationally symmetric natural convection loop is established,

2) the agreement of measured and predicted time dependent temperature profiles.

The experiments were not planned on the basis of similarity theory, but rather for the creation of intensive natural convection flows to allow validation of the physical models used in THERMIX-KONVEK.

Figures 5.9-a and 5.9-b show typical results for a natural convection experiment using air at 30 bars. For the natural convection experiments, the basic procedure was such that temperature differences caused by radial heat removal (from the bed previously heated to a uniform temperature by forced convection) set in motion a macroscopic internal natural convection loop. At the start of the transient when the bed was isolated and the water jacket held at low temperature (~30°C), the edge of the bed cooled down by conduction and radiation due to the water cooling of the outer pressure shell. The resulting density differences set up a free convection flow that resulted in downward gas flow along

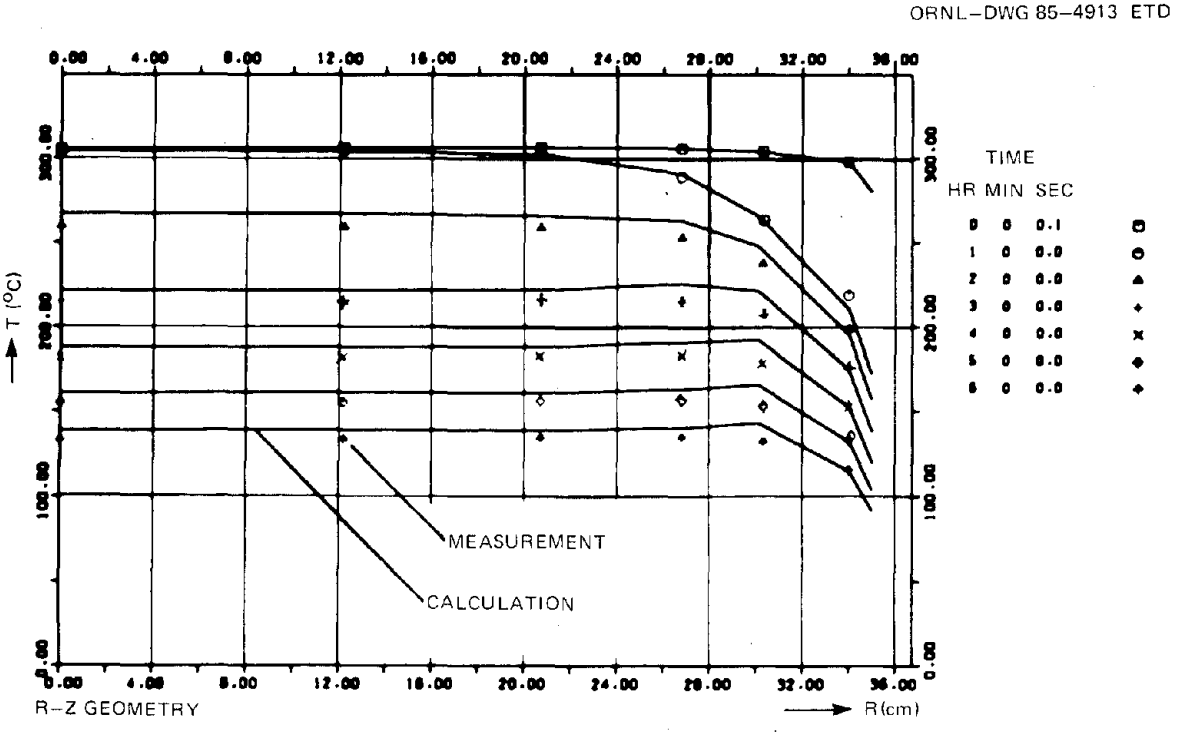

Fig. 5.9-a. Comparison of calculated and measured radial temperature profiles during natural convection experiment. (Figure taken from Ref. 3.)

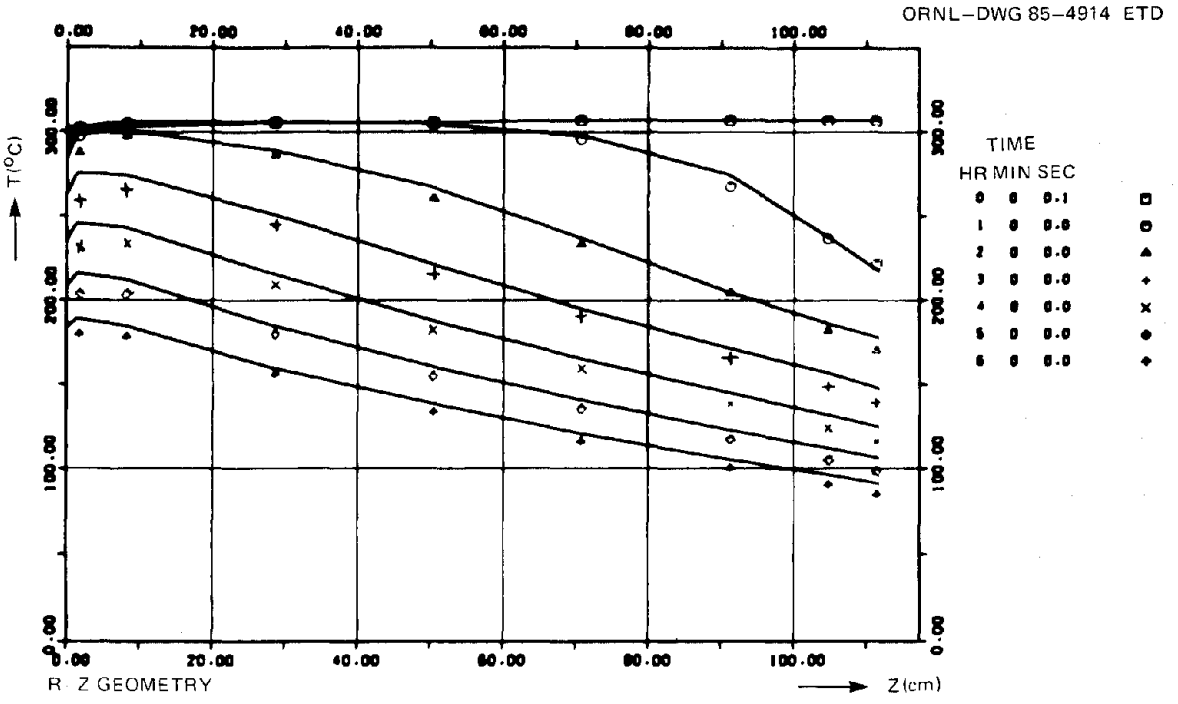

Fig. 5.9-b. Comparison of calculated and measured axial temperature profiles during natural convection experiment. (Figure taken from Ref. 3.)

the cold wall of the steel vessel and in the outer regions of the bed and upward gas flow in the bed interior. Measurements reported in Ref. 3 showed a virtually rotationally symmetric temperature distribution during the tests. Deviations from the radial symmetry occurred only in the upper region of the bed.

The air cooled in the region adjacent to the wall enters the bed at the bottom and this brings about a continuous cooling from the bottom to the top (see Fig. 5.9-b). Since there is little radial temperature gradient in the center, no heat transport takes place in this direction. However, in the peripheral region, because of the large temperature gradient, there is a considerable transport of heat by conduction and radiation.

Good agreement between calculation and measurement was obtained over a range of pressures (1 to 30 bars) and with both air and helium, confirming the appropriateness of the THERMIX-KONVEK model. In comparing the pressurized air and helium experiments, an interesting but

expected result was the observation that at the same pressure, in spite of the lower circulation flows with helium (because of the lower density), the measured rate of heat transport out of the bed into the cooling water was higher. This was due to the higher specific heat and thermal conductivity of the helium.

The relative effects of convection and of conduction/radiation were analytically compared with measured results for a natural convection experiment involving air at 30 bars. Figure 5.10 shows that both are important under these conditions. With increasing convective flow the effect of the effective thermal conductivity, λ_e, becomes limited to the region of the bed adjacent to the wall which is characterized by a high radial temperature gradient.

Experiments to investigate the effective conductivity of the bed of steel spheres under depressurized conditions (1 bar air or 1.5 bar helium) at temperatures up to 300°C were also conducted. At these conditions, according to Rayleigh theory, the density differences established by the radial heat transport to the vessel wall were below the critical values required for inception of natural convection. Therefore, heat

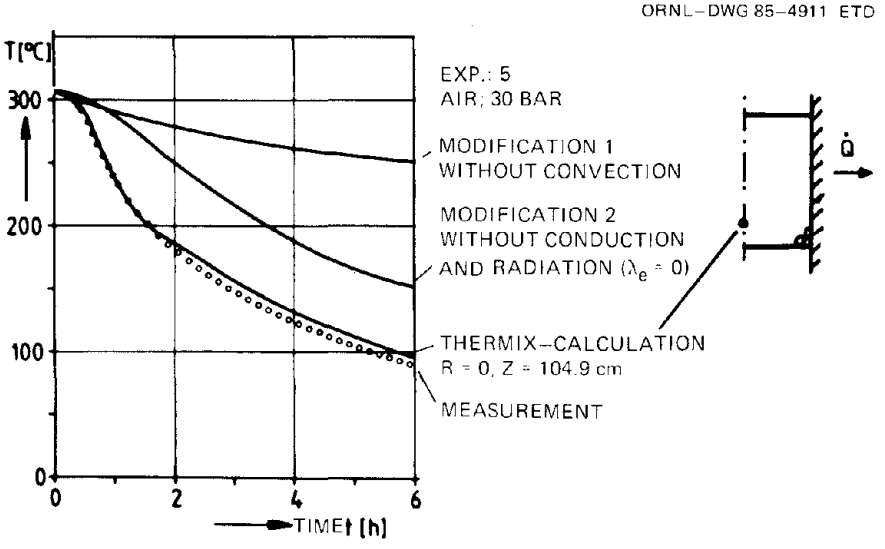

Fig. 5.10. Measured and calculated time dependent temperature near bottom of bed of steel spheres during a natural convection experiment. (Figure taken from Ref. 3.)

transport was limited to conduction and radiation. Results of these experiments led to the modified correlation for λ_e by Schürenkrämer for a bed of 6 cm diameter graphite pebbles which is presented in Sect. 5.1.1.

Experiments were also performed to examine unstable temperature stratification. In HTRs, unstable temperature stratification occurs with a downflow core if the coolant flow is interrupted. For this condition, cool gas is above the hot gas in an unstable configuration. In the experiment, this condition was established by initially heating the bed to a uniform temperature and then by establishing an axial temperature gradient in the bed by a forced downward flow of cool gas. When this flow was stopped, an unstable temperature stratification existed. The objective of this experiment was to determine if directionally stable natural convection flow is established and whether the solid temperatures can be accurately predicted with THERMIX-KONVEK. Results of this experiment are shown in Figures 5.11-a and 5.11-b. In this experiment, after initially heating the bed to a uniform temperature of 300°C

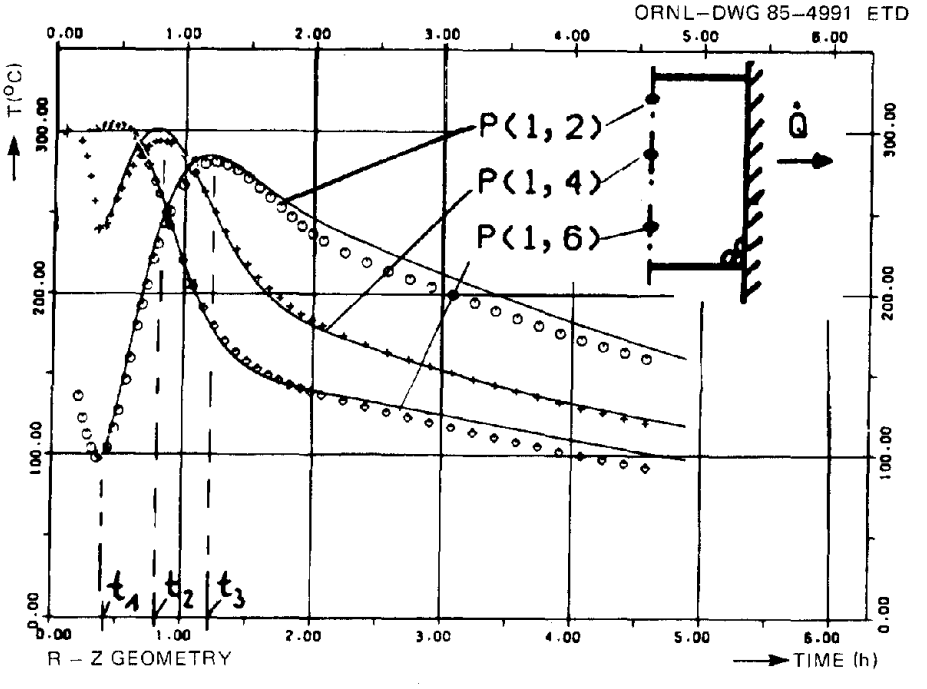

Fig. 5.11-a. Comparison of calculated and measured results for temperatures along vertical axis of test section during experiment initially involving unstable gas temperature stratification. (Figure taken from Ref. 3.)

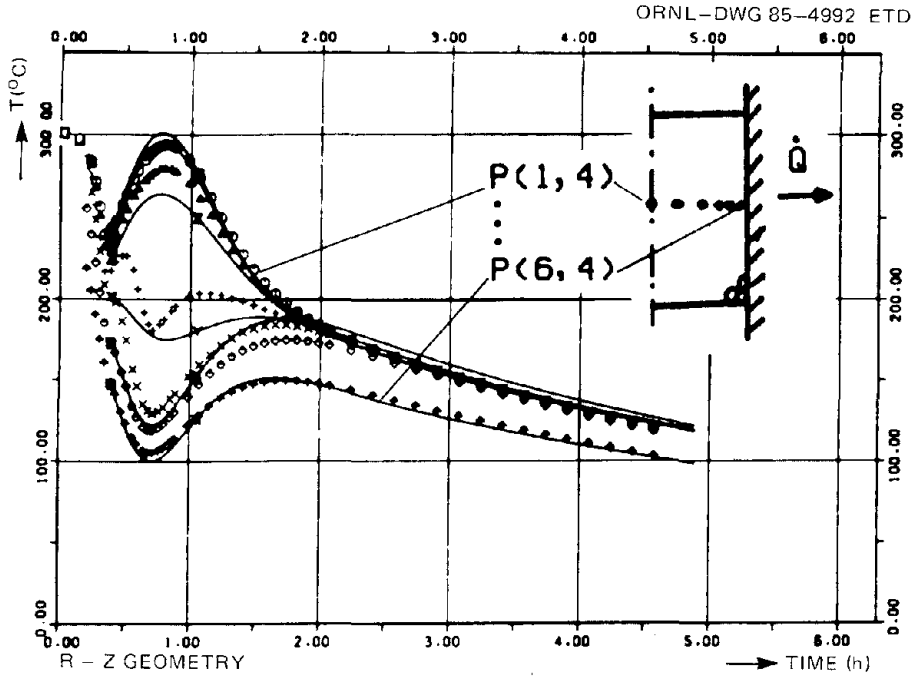

Fig. 5.11-b. Comparison of calculated and measured results for radial temperatures during experiment initially involving unstable gas temperature stratification. (Figure taken from Ref. 3.)

by forced convection of hot gas, a forced downward flow of cool gas was introduced for 0.39 h. This established an axial temperature gradient in the bed. With interruption of this forced flow of cold gas (at t_1 = 0.39 hr), the spheres near the boundary initially continue to cool down because of the radial heat removal from the bed by the cooling of the vessel wall by cool water flowing in the water jacket. The spheres in the upper region of the bed along the vertical axis begin to heat up due to the macroscopic free convection which transports heat upward from the lower region of the bed which is still at high temperatures. The transport of heat from the bed interior then results in a reheating of the boundary spheres. The comparisons of predicted and measured results (Figs. 5.11-a and 5.11-b) show fair agreement but are somewhat misleading because measured temperatures at the same r-z coordinates have been averaged azimuthally. In fact significant azimuthal deviations (up to 100°C) occurred during the test.

Another experiment examined superposition of natural convection and forced downward flow under pressurized conditions (30 bars, air).

First, an intensive natural convection flow was established in the bed as in the natural convection cooldown experiments. Then a flow of cold gas was injected from the top so that the free upward flow and the forced downward flow were in opposition. An example of application in the HTR is the delayed startup of active decay heat removal operation with forced downward coolant flow.

In this experiment, with this superposition of forced and natural flow, rotational symmetry was not achieved, and thus the 2-D THERMIX-KONVEK code could not reproduce the results. The deviations from rotational symmetry resulted from the fact that the downward forced flow of cold gas favored the cooler regions of the bed which presented the lower flow resistance (due to the lower viscosity and the higher gas density). Slight deviations from rotational symmetry which developed during the period of the test which involved only natural convection provided the starting point for this asymmetric behavior. Further, one would not expect to predict the asymmetry with a 3-D THERMIX-KONVEK representation because factors causing deviations from rotational symmetry (for example, deviations from a uniform fill arrangement of the pebbles) are not explicitly predictable and therefore could not be accounted for in the input to the 3-D model.

Further experiments were performed on the large research rig to investigate dispersive heat transport and to compare measured data with THERMIX-KONVEK predictions. Reference 5 discusses these experiments and compares code predictions with measured data for a steady state temperature profile under forced flow conditions. In these experiments the steady state temperature profile was established in the bed of steel spheres (1.9 cm diam) by injecting a "point source" of cooler air (in the range of 140 to 200°C) into the bed of spheres while a main stream flow of hot air (~270°C) was forced downward through the bed. Figure 5.12 shows the test section with the cool air injection pipe in place. Several experiments were performed using different ratios of cold to hot air flow and different cold air temperatures. Flows were sufficient so that the dispersive thermal conductivity $\lambda_f \frac{Pe}{K}$ of the gas dominated the thermal conductivity term λ_e of the solid. Thus dispersion and convection were the major factors in determining the heat transport in

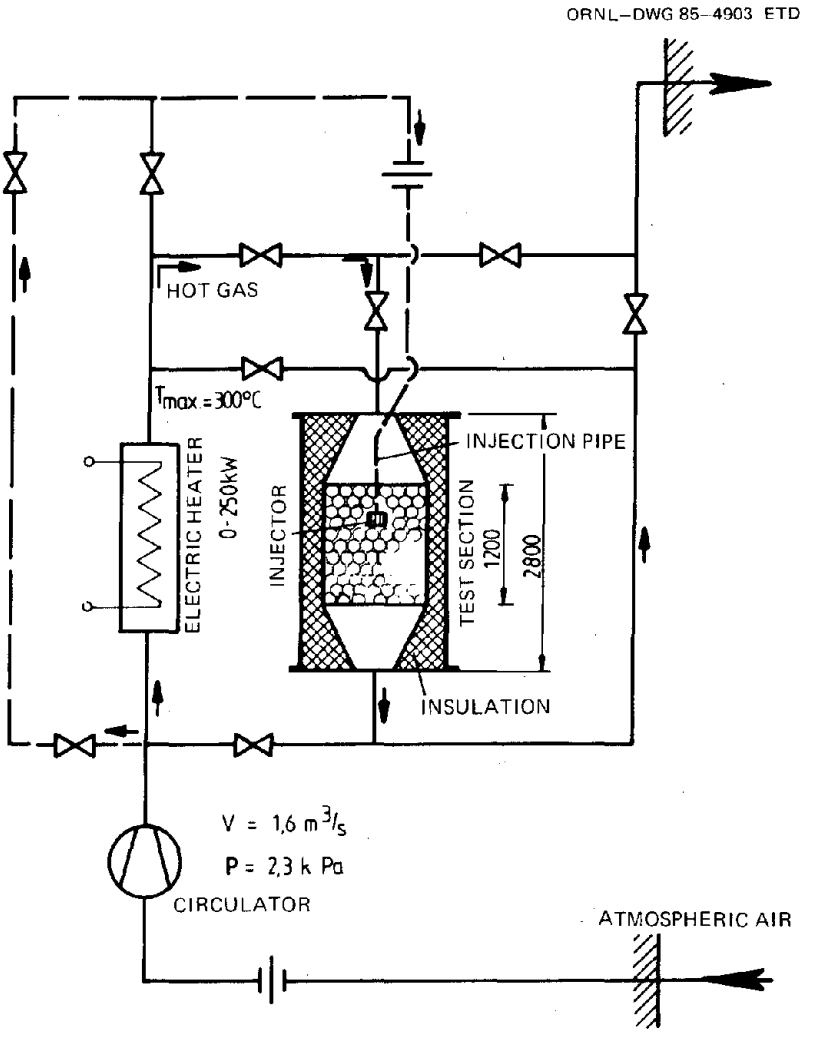

Fig. 5.12. Schematic of large research rig with cold gas injector installed in test section. (Figure taken from Ref. 5.)

the bed. In comparing measured results with code predictions the dimensionless temperature difference

$$\Theta\,(r,t) = \frac{T_{\text{hot gas}} - T_{\text{bed}}(r,t)}{T_{\text{hot gas}} - T_{\text{cold gas}}}$$

is plotted against bed radius for selected axial planes. Results of a typical experiment compared with code predictions are shown in Fig. 5.13. In general, the calculations show good agreement with the measured results verifying the dispersive model.

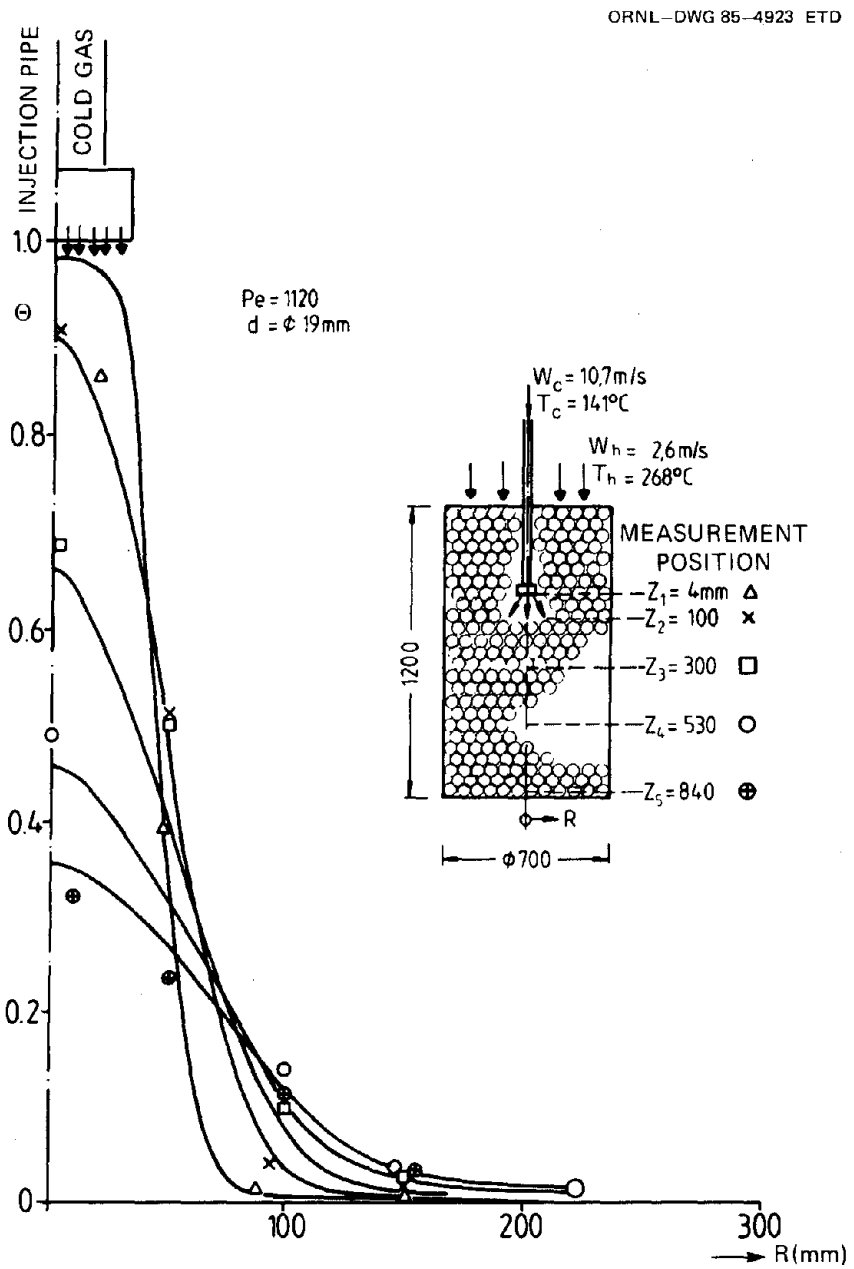

Fig. 5.13. Comparison of calculated and measured profile with "point source" of cold gas introduced into a pebble bed heated by forced convection. (Figure taken from Ref. 5.)

5.2 Applicability to the U.S. Pebble Bed Modular HTR

THERMIX-KONVEK is appropriate for steady state and transient analyses of the U.S. pebble bed modular HTR. The primary heat transport mechanisms in the core, reflectors, reactor vessel, and reactor cavity

out to the cavity cooling system can be modeled. Probably the major virtue of the code is its ability to calculate the two-dimensional mass flow and temperature fields in the pebble bed region for a full range of conditions, even as the reactor is experiencing a transient. It is the only available code for performing such analyses. THERMIX-KONVEK can perform these calculations for conditions ranging from forced to natural convection flow and for pressures ranging from depressurized conditions to conditions involving above normal operating pressures.

THERMIX-KONVEK has been verified in small-to-medium scale out-of-pile tests for a range of conditions including depressurized cooldown, natural and forced convection. Comparison with measured data has verified the simplifying assumptions used in the code such as semi-homogeneity of the pebble bed, quasi-static calculation of the fluid side, and disregard of acceleration forces. While these tests have been extensive, they have not covered the complete range of conditions which are representative of hypothetical accidents for pebble bed modular HTRs. Summarizing the experimental work discussed in Sect. 5.1 of this report:

- The effective conductivity (λ_e) of a bed of spheres has been experimentally investigated by Breitbach and Barthels (Ref. 11) for a bed of (unirradiated) graphite spheres (4 cm diam) over the temperature range of 200°C to 1500°C and for ZrO_2 (4.5 cm diam) low emittance spheres over the range 400-1000°C. Results of these experiments were used to modify theoretical models. These modified models were then used to predict λ_e for a packed bed of graphite pebbles (6 cm diam) over the temperature range of 1000 to 2500°C assuming a temperature independent value for matrix graphite conductivity.
- Other investigations by Schürenkrämer (Ref. 3) and by Robold (Ref. 10) also led to predictions of λ_e for 6 cm graphite pebbles. Robold further investigated the behavior of λ_e near the reflector wall. Both investigators presented predictions of λ_e for 6 cm graphite pebbles for selected matrix graphite conductivities, based on theoretical models.
- Experiments at KFA's small research rig which contained a packed bed (40 cm high by 24.8 cm diam) of steatite (1 cm diam) spheres

validated THERMIX-KONVEK prediction for conditions involving natural convection heat transport and radiation/conduction heat transport with bed temperatures up to 100°C and pressures ranging from 1 to 20 bar (using air, N_2 and CO_2).

- Experiments at KFA's large research rig which contained a packed bed (120 cm high by 70 cm diam) of steel spheres (1.9 cm diam) validated THERMIX-KONVEK predictions for conditions involving natural convection, dispersion, and radiation/conduction heat transport. Tests were done at temperatures up to 300°C and at pressure ranging from 1 to 36 bars (with air and helium coolant).

  Results of experiments at 1 bar pressure (in which radiation and conduction dominated) were well predicted by THERMIX-KONVEK. Also, results of natural convection experiments were well predicted by THERMIX-KONVEK. Results of experiments initialized with unstable temperature stratification were not predicted very well with THERMIX-KONVEK due to significant azimuthal deviations which occurred during the experiment. Fair agreement with the predictions by THERMIX-KONVEK could be obtained only by comparing code predictions with azimuthally averaged values of the measured temperatures. Another experiment involving superposition of downward forced flow and natural convection flow resulted in highly asymmetric temperature distributions. These azimuthal deviations obviously could not be predicted with the 2-D THERMIX-KONVEK (and resulted from physical conditions in the bed which probably cannot be precisely anticipated for modeling even with a 3-D model). Experiments were conducted with forced gas flow to test the modeling of dispersive heat transport in the gas and computed results agreed well with measurements.

Because of the above fairly extensive and fairly successful validation efforts in small-scale, out-of-pile tests, the major area of validation which is currently lacking involves more prototypic reactor conditions involving, for example, the following

- a packed bed of irradiated 6 cm diam graphite fuel pebbles (of varying degrees of irradiation)
- bed temperatures ranging up to somewhat higher than 1600°C

- natural convection in helium at temperatures up to ~1200°C at a pressure of 70 bar and somewhat higher
- temperatures of the reactor vessel internals (e.g. upper head region)
- reactivity changes (to validate KINEX neutron kinetics module).

5.3 Recommended Additional Validation

It is recommended that the next step in code validation focus on conditions more typical of actual reactor operation and of hypothetical accidents than have been possible with the tests performed to date at KFA. This could progress as discussed in the following sections.

5.3.1 Comparison of THERMIX predictions with measured plant data

As the next phase in THERMIX validation, code predictions should be compared with measured steady state and transient operating data from both THTR and AVR. This would test the accuracy of THERMIX-KONVEK-KINEX over a range of actual conditions of temperature, pressure, fluence and internal heat generation rate not covered in the smaller scale out-of-pile tests. While measured information will not be as extensive as would be obtained from a specially designed test facility, experience has shown (for example, Refs. 14-16) that significant information relative to validity of analytical tools under reactor conditions can be obtained by such comparisons. With the understanding derived from these activities, it is often possible to plan special tests or measurements at the reactors which can be performed with minimal disruption to the plant that can investigate some key feature for further validation of code predictions.

5.3.2 Sensitivity analyses followed by potential special tests

This effort would involve accident studies of modular pebble bed HTRs including sensitivity analyses to examine the importance that certain parameters have on predicted results. Then, for those conditions for which it is judged that the existing validation of THERMIX-KONVEK-KINEX is insufficient (either by comparison with experimental data from

KFA's special test facilities, or by comparison with THTR and AVR operating data) special tests can be planned and conducted.

5.3.3 Comparison of THERMIX results with other analytical results to test special features

As is noted in Sect. 4.1, buttresses used to provide channels for control rods could not be modeled with the two dimensional THERMIX code. The effect of neglecting buttresses should be examined by comparison of THERMIX predictions with a special 3-D calculation — for example, with HEATING-6 (Ref. 17) for depressurized conditions. (HEATING-6 can treat radiation and conduction, but not natural convection so the comparison necessarily must be done for depressurized conditions where natural convection is neglegible.)

Other special tests against analytical tools may be identified in the future.

6. SUGGESTED FURTHER INVESTIGATIONS FOR MODULAR HTRs

As a result of ORNL's effort to model the pebble bed modular HTR and the initial trial calculations, further analyses are suggested to examine more closely the fuel, vessel and vessel internals temperatures during normal and accident conditions. In summary, these are

- investigate the effect of control rod channels and coolant channels on the effective conductivity of the side reflector blocks and the resultant impact on fuel temperatures during core heatup events (Note: this is a generic question also appropriate to prismatic fueled modular HTRs),
- investigate the sensitivity of fuel and vessel temperatures under accident conditions to
  - reflector graphite conductivity (irradiated and unirradiated)
  - emissivities of steel and graphite surfaces
  - effective conductivity of the core
- investigate temperatures in the top reflector (which contains no coolant passages) accounting for heat generation by neutron and gamma heating,
- investigate the accuracy of the THERMIX-KONVEK modeling of
  - heat transport to the upper vessel head
  - heat transport to the top reflector
  - heat transport by free convection in the vertical annular gaps such as in the helium space between the side reflector and the reactor vessel. THERMIX accounts for this heat transport using the so called "thermal conduction by convection" which correlates a "conductivity" for the gap with the gas conductivity and the Grashof and Prandtl numbers.

The first two items also apply to prismatic fueled modular HTRs. Note that conditions which can be considered conservative for calculation of fuel temperature (for example assuming a low value for reflector graphite conductivity) are not conservative from the viewpoint of vessel temperature.

7. RECOMMENDED CODE DEVELOPMENT WORK

While THERMIX-KONVEK is the best available code for analysis of pebble bed HTRs, there are several characteristics of the code and its associated documentation which could be addressed to improve THERMIX-KONVEK. These code improvements are in the general areas of (a) improved documentation, (b) improved user interface, and (c) technical improvements. The following paragraphs present a brief description of desired enhancements to the code.

- Documentation:

1. Update of the User's Manual to provide concise and complete descriptions of each of the input variables in the current version;
2. Translation of the output labels and warning statements from German to English;
3. Translation of the code comment cards from German to English;
4. Generation of a one page description of each subroutine in the code which would describe the subroutine input and output variables as well as a very brief description of the calculation performed by the subroutine;
5. Generation of an English language THERMIX-KONVEK-KINEX Reference Manual, which would provide the technical basis for the calculations performed by the code. This document would include the subroutine descriptions from item 4 above, as well as descriptions of constitutive relationships, mathematical techniques, etc.

- Code Improvements - User Interface (I/O):

The following code improvements would enhance the code's utility:

1. Supplement the current fixed format input technique with a variable format or name list format input preprocessor. With the current fixed format input it is common for two numbers to be placed side by side on the input data cards with no intervening blank spaces — thus making it difficult to locate specific variables within the input data file. Use of a preprocessor would ease the task of generating input for the code while retaining the ability to transmit input decks between facilities for trouble shooting and other examinations. The input data processor should also check the

THERMIX and KONVEK input data streams for inconsistencies and common errors. This would save much time during the model development stage, by flagging errors early, as well as providing the user assistance in locating syntax errors in the input data.

2. The code currently requires that two distinct models be input (one for THERMIX and one for KONVEK). Since some of the information within these two models is either redundant or could be synthesized from the information input for the other module, it is recommended that an internal THERMIX/KONVEK interface be constructed which would allow KONVEK to utilize THERMIX input data where redundant input requirements exist, and to automatically synthesize as much of its input data requirements as is possible from the THERMIX input data.
3. The general procedure for running THERMIX-KONVEK is to generate a steady state input data deck, execute the code (which generates and saves the steady state temperature distribution throughout the system), modify the input data deck to reflect the desired transient conditions and to incorporate the initial temperature distribution determined by the steady state run, and finally execute THERMIX-KONVEK for the transient. The modification of the steady state input data deck to set up a transient case can lead to errors due to the necessity of modifying variables which are located on different cards in the THERMIX and KONVEK input data streams. The input data formats should be restructured to group all of the variables which must or might be modified when converting from a steady state run to a transient run in one well defined region of the input data string.
4. A graphics package should be generated which couples with THERMIX-KONVEK to efficiently display computed results.

- Code Improvements - Technical:

The following technical modifications should be considered:

1. Incorporation of "horizontal flow tubes" or channels in the model. This modification is necessary to facilitate a realistic geometric treatment of the ducting of gas through the reflector into the upper plenum in the U.S. pebble bed modular HTR concept.

2. The code currently performs an iteration at each time step to determine the two dimensional solid body temperature distribution and iterates each time step to determine the two dimensional flow and temperature fields. The amount of time consumed for each type of iteration should be determined, and other methods — such as sparse, banded matrix solution techniques which potentially could speed up code execution should be examined.
3. The accuracy of the THERMIX solution for the temperature distribution within the pebble should be examined. In the trial calculations reported here, while the expected temperature profile from pebble centerpoint to pebble surface was obtained at initial steady state conditions, results for decay power levels at depressurized conditions were questionable. While the code did predict a very low ΔT of only 2 to 3°C from pebble centerpoint to surface as expected, the temperature profile in some cases showed a slightly higher temperature (of approximately 1°C) in the fourth shell (next to the outer shell) of the five shells in the pebble model. No plausible explanation for this phenomenon could be identified. The problem may be related to an apparent error in a relationship written in Reference 2. This reference presents the conservation of energy equation for the temperature distribution within the pebble (equation 8 in Ref. 2); however, in Ref. 2, $\dot{Q}_{\lambda s}$ and $\dot{Q}_k$ (see Section 2.3 for their definition) are added to the nuclear power generation which is internal to the pebble. A review showed that $\dot{Q}_{\lambda s}$ and $\dot{Q}_k$ represent rates of heat transfer from the pebble surface and not rates of heat generation internal to the pebble (see equation 2 and Section 2.3 of this report).

8. REFERENCES

1. K. Petersen, Zur Sicherheitskonzeption des Hochtemperaturreaktors mit natürlicher Wärmeableitung aus dem Kern im Störfall, Jül-1972, October 1983.

2. J. Banaschek, Berechnungsmethoden und Analysen zum dynamischen Verhalten von Kraftwerksanlagen mit Hochtemperaturreaktor, Jül-1841, April 1983.

3. M. Schürenkrämer, Theoretische und experimentelle Untersuchungen der Naturkonvektion im Kern des Kugelhaufen-Hochtemperaturreaktors, Jül-1912, April 1984.

4. Sicherheitstechnische Regel des KTA, Auslegung der Reaktorkerne von gasgekühlten Hochtemperaturreaktoren, Teil 3: Reibungsdruckverlust in Kugelhaufen, KTA 3102.3, March 1981.

5. M. Schürenkrämer and H. Barthels, Experimentelle Untersuchungen zur Thermohydraulik in Kugelschüttungen im Vergleich mit dem Rechenprogramm THERMIX-2D, Die Untersuchung des dispersiven Wärmetransportes am Beispiel einer Kaltgassträhne, Jül-1839, April 1983.

6. Sicherheitstechnische Regel des KTA, Auslegung der Reaktorkerne von gaskühlten Hochtemperaturreaktoren Teil 1: Berechnung der Helium-Stoffwerke, KTA 3102.1, June 1978.

7. Sicherheitstechnische Regel des KTA, Auslegung der Reaktorkerne von gasgekühlten Hochtemperaturreaktoren, Teil 2: Wärmeübergang im Kugelhaufen, KTA 3102.2, November, 1982.

8. R. M. Harrington et al., Simulation of the Thermal Response of the 250 MW_t Modular HTR during Hypothetical Uncontrolled Heatup Accidents, presented at the IAEA Specialist's Meeting on Safety and Accident Analyses for Gas-Cooled Reactors, May 13-15, 1985, Oak Ridge, Tennessee.

9. R. F. Benenati, C. B. Brosilow, Void Fraction Distribution in Beds of Spheres, A.I.Ch.E. Journal 8 (1962) No. 3, p. 359-361.

10. K. Robold, Wärmetransport im Inneren und in der Randzone von Kungelschüttengen, Jül-1996, July 1982.

11. G. Breitbach and H. Barthels, The Radiant Heat Transfer in the High Temperature Reactor Core after Failure of the Afterheat Removal Systems, Nuclear Technology, Vol. 49, August 1980, pp. 392-399.

12. L. Binkele, Ein Verfahren zur Bestimmung der Wärmeleitfähigkeit von neutronbestrahlten Graphiten bei Temperaturen zwischen 50 und 1000°C, Jül-1096-RW, August 1974.

13. K. Verfondern, Experimentelle Überprüfung des Thermohydraulik Programms THERMIX und rechnerische Analyse der Transienten Temperatur- und Strömungsfelder im Corebereich des THTR-Reaktors nach Ausfall der NWA, (Interner Bericht) KFA-IRE-IB-13/78, October 1978.

14. S. J. Ball, J. C. Cleveland, R. M. Harrington, "ORNL's NRC-Sponsored HTGR Safety and Licensing Analysis Activities for Fort St. Vrain and Advanced Reactors," Proceedings of the IAEA Specialist's Meeting on Safety and Accident Analysis for Gas Cooled Reactors, Oak Ridge, TN, May 13-15, 1985.

15. ORNL HTGR Code Assessment Report, February 28, 1985.

16. J. C. Cleveland, "ORNL Analysis of AVR Performance and Safety," Proceedings of the IAEA Specialists' Meeting of Safety and Accident Analysis for Gas-Cooled Reactors, Oak Ridge, TN, May 13-15, 1985.

17. D. C. Elrod et al., HEATING-6: A Multidimensional Heat Conduction Analysis Code with the Finite Difference Formulation, included in "SCALE: A Modular Code System for Performing Standardized Computer Analyses for Licensing Evaluation," ORNL/NUREG/CSD-2.

NUREG/CR-4694
ORNL/TM-9905
Distribution Category R8

Internal Distribution

1. S. J. Ball
2-10. J. C. Cleveland
11. T. E. Cole
12. W. G. Craddick
13-17. S. R. Greene
18. R. M. Harrington
19. J. E. Jones Jr.
20. P. R. Kasten
21. T. S. Kress
22. A. P. Malinauskas
23. D. L. Moses
24. J. P. Sanders
25. H. E. Trammell
26. D. R. Vondy
27. R. P. Wichner
28. B. A. Worley
39. ORNL Patent Office
30-31. Laboratory Records Department
32. Laboratory Records, RC
33. Central Research Library
34. Document Reference Section

External Distribution

35. Ronald B. Foulds, Division of Accident Evaluation, RES, MS-1130SS, U.S. Nuclear Regulatory Commission, Washington, DC 20555
36. Richard E. Ireland, U.S. Nuclear Regulatory Commission, Region 4, 611 Ryan Plaza Drive, Suite 1000, Arlington, TX 76011
37-41. Thomas L. King, Office of Nuclear Regulatory Regulation, Mail Stop 216, U.S. Nuclear Regulatory Commission, Washington, DC 20555
42. N. Kirch, HTA-Projekt, Kernforschungsanlage, Jülich GmbH, Postfach 1913, D-5170, Jülich 1, Federal Republic of Germany
43. Peter G. Kroeger, HTGR Safety Division, Department of Nuclear Energy, Brookhaven National Laboratory, Upton, NY 11973
44. K. Krüger, Department Leader, Reactor Analysis and Experiments, Arbeitsgemeinschaft Versuchs Reaktor AVR-GmbH, D-5170 Jülich, Federal Republic of Germany
45. W. Rehm, Institut für Nukleare Sicherheitsforschung, Kernforschungsanlage, Postfach 1913, D-5170 Jülich, Federal Republic of Germany
46. E. Teuchert, Institut für Reaktorentwicklung IRE/L, Kernforschungsanlage, Postfach 1913, D-5170 Jülich, Federal Republic of Germany
47. G. J. VanTuyle, HTGR Safety Division, Department of Nuclear Energy, Brookhaven National Laboratory, Upton, NY 11973
48. Peter M. Williams, Division of Safety Technology, Research and Standards Coordination Branch, U.S. Nuclear Regulatory Commission, MS-P846, Washington, DC 20555
49. Dr. L. Wolf, Section Leader, Reactor Physics Analysis, Institut für Reaktorentwicklung, Kernforschungsanlage-Jülich, D-5170 Jülich, Federal Republic of Germany

50. Office of Assistant Manager for Energy Research and Development, Department of Energy, ORO, Oak Ridge, TN 37831
51-52. Technical Information Center, U.S. Department of Energy, Oak Ridge, TN 37831
53-237. Given distribution as shown in Category R8 (10 — NTIS)